Available online at www.sciencedirect.com

ScienceDirect

Geochimica et Cosmochimica Acta 209 (2017) 320–342

Geochimica et Cosmochimica Acta

www.elsevier.com/locate/gca

Calcium and strontium isotope fractionation during precipitation from aqueous solutions as a function of temperature and reaction rate; II. Aragonite

Mahmoud AlKhatib, Anton Eisenhauer *

GEOMAR Helmholtz-Zentrum für Ozeanforschung Kiel, 24148 Kiel, Wischhofstr. 1-3, Germany

Received 16 May 2016; accepted in revised form 10 April 2017; Available online 25 April 2017

Abstract

In order to study Strontium (Sr) partitioning and isotope fractionation of Sr and Calcium (Ca) in aragonite we performed precipitation experiments decoupling temperature and precipitation rates (R^*, μmol/m^2 h) in the interval of about 2.3–4.5 μmol/m^2 h. Aragonite is the only pure solid phase precipitated from a stirred solutions exposed to an atmosphere of NH_3 and CO_2 gases throughout the spontaneous decomposition of $(NH_4)_2CO_3$. The order of reaction with respect to Ca ions is one and independent of temperature. However, the order of reaction with respect to the dissolved inorganic carbon (DIC) is temperature dependent and decreases from three via two to one as temperature increases from 12.5 and 25.0 to 37.5 °C, respectively. Strontium distribution coefficient (D_{Sr}) increases with decreasing temperature. However, R^* responds differently depending on the initial Sr/Ca concentration and temperature: at 37.5 °C D_{Sr} increase as a function of increasing R^* but decrease for 12.5 and 25 °C. Not seen at 12.5 and 37.5 °C but at 25 °C the D_{Sr}-R^* gradient is also changing sign depending on the initial Sr/Ca ratio. Magnesium (Mg) adsorption coefficient between aragonite and aqueous solution (D_{Mg}) decreases with temperature but increases with R^* in the range of 2.4–3.8 μmol/m^2 h. Strontium isotope fractionation ($\Delta^{88/86}Sr_{aragonite\text{-}aq}$) follows the kinetic type of fractionation and become increasingly negative as a function of R^* for all temperatures. In contrast Ca isotope fractionation ($\Delta^{44/40}Ca_{aragonite\text{-}aq}$) shows a different behavior than the Sr isotopes. At low temperatures (12.5 and 25 °C) Ca isotope fractionation ($\Delta^{44/40}Ca_{aragonite\text{-}aq}$) becomes positive as a function of R^*. In contrast, at 37.5 °C and as a function of increasing R^* the $\Delta^{44/40}Ca_{aragonite\text{-}aq}$ show a Sr type like behavior and becomes increasingly negative. Concerning both the discrepant behavior of D_{Sr} as a function of temperature as well as for the Ca isotope fractionation as a function of temperature we infer that the switch of sign in the trace element partitioning as well as in the direction of the Ca isotope fractionation is probably due to the switch of complexation from a Ca^{2+}-NH_3 complexation at and below 25 °C to an Ca^{2+}-H_2O aquacomplex at 37.5 °C. The D_{Sr}–$\Delta^{88/86}Sr_{calcite\text{-}aq}$ correlation for calcite is independent of temperature in contrast to aragonite. We interpreted the strong D_{Sr}-temperature dependency of aragonite, the smaller range of Sr isotope fractionation as well as the shallower $\Delta^{88/86}Sr_{calcite\text{-}aq}$–$R^*$ gradients to be a consequence of the increased aragonite solubility and the "Mg blocking effect". In contrast to Sr the Ca isotope fractionation values in calcite and aragonite depend both on the complexation in solution and independent on polymorphism.

Keywords: Aragonite; Calcite; Strontium; Magnesium; Calcium; Isotopes; Fractionation; Blocking effect

1. INTRODUCTION

From the three main calcium carbonate ($CaCO_3$) polymorphs, aragonite, calcite and vaterite, aragonite is

* Corresponding author.
E-mail address: aeisenhauer@geomar.de (A. Eisenhauer).

http://dx.doi.org/10.1016/j.gca.2017.04.012
0016-7037/

the second most abundant in the marine environment (c.f. Morse and Mackenzie, 1990; Morse et al., 2007) where it is produced either by uni- and multicellular calcifying organisms or by inorganic precipitation processes. Aragonite preferentially incorporates alkaline-earth metals like Sr^{2+} and Ba^{2+} as trace elements of which their concentrations and ratios reflect the chemical conditions in the adjacent water during mineral precipitation (Eisenhauer et al., 2009). Being of particular interest in paleoceanography for the reconstruction of seawater temperatures Sr/Ca ratios usually expressed as the distribution coefficient D_{Sr} ($[Sr/Ca]_{CC}/[Sr/Ca]_{SW}$; CC = Calcium carbonate, SW = Seawater) shows an inverse relationship with temperature during calcification (c.f. Weber, 1973; Smith et al., 1979; De Villiers et al., 1994). In biologically mediated $CaCO_3$ the D_{Sr} values tend to be different from the inorganic thermodynamically expected value, an effect generally known as the "vital effect". The latter effect reflects the physiological control of the calcifying organisms and the species dependent biomineralization pathways for $CaCO_3$ precipitation. The Sr/Ca ratios in coral skeletons are not only dependent on temperature (c.f. Beck et al., 1992) but also on the Sr/Ca ratio in seawater itself which can also be used to reconstruct the composition of paleo-water as well as the diagenetic reactions that involve carbonate sediments (Scherer and Seitz, 1980; Enmar et al., 2000). Many experimental studies have been carried out to examine the kinetics of precipitating aragonite (e.g. c.f. Kinsman and Holland, 1969; Burton and Walter, 1987; Dietzel et al., 2004; Gaetani and Cohen, 2006; Gabitov et al., 2008; Niedermayr et al., 2013; Gabitov, 2013; Kim et al., 2014), however most of these studies focused on the effect of temperature on the Sr/Ca ratio in aragonite in terms of D_{Sr} showing that these values decrease with increasing temperature.

Although it has been discussed that Ca ($\delta^{44/40}Ca$) and Sr ($\delta^{88/86}Sr$) isotopes measured in calcite and aragonite may be used to reconstruct environmental conditions from the adjacent seawater (Gussone et al., 2003; Fantle and Higgins, 2014) research focused mainly on biologically precipitated calcite and aragonite. Only a few studies are available concerning Ca isotope fractionation during inorganic aragonite precipitation (c.f. Gussone et al., 2003). Even more, to our knowledge no study is yet available about Sr isotope fractionation during inorganic aragonite precipitation.

This lack of data and information is the impetus for this study, in which we precipitated aragonite at three different temperatures (12.5, 25.0 and 37.5 ± 0.2 °C) from buffered aqueous ammonium by controlled diffusion of CO_2 (g) and NH_3 (g) with a wide range of R^*. Following this experimental approach we are able to study the dependency of the precipitation from the rate (R^*) and the temperature (T) both probably the two most important parameters influencing $CaCO_3$ precipitation. Note, this study extents and completes a similar study we have performed concerning calcite (AlKhatib and Eisenhauer, 2017). Experimental setup, chemical solutions (except for the Mg concentration) and equations are identical with this earlier companion study.

2. MATERIAL AND METHODS

2.1. Materials and experimental setup

Except for the molar Mg/Ca ratio which was set to be 3:1 the solutions as well as the experiments performed to precipitate aragonite is completely based on the earlier set up as described in AlKhatib and Eisenhauer (2017), Fig. 1). The [Mg/Ca] ratio was set to 3.1 because any Mg/Ca above about 2:1 guarantees the precipitation of aragonite instead of calcite. This is for example the case in the ocean where the Mg/Ca ratio shows a molar ratio of 5.2.

In brief two main sets of solutions were prepared to produce aragonite in an ammonium buffered solutions (NH_4/NH_3) at three different temperatures 12.5, 25.0 and 37.5 °C (±0.2 °C). The first set is composed of 0.395 M NH_4Cl, 10.0 mM $CaCl_2$ and 0.10 mM $SrCl_2$. The second solution shows the same composition except for $SrCl_2$ set to be 0.050 mM. In order to verify differences in chemical composition three solutions were prepared differently either containing 15 or 150 mM [Ca], respectively: Solution No. 4 is composed of 0.395 M NH_4Cl, 19.84 mM $CaCl_2$ and 0.11 mM $SrCl_2$, solution No. 7 is composed of 0.395 M NH_4Cl, 149 mM $CaCl_2$ and 0.11 mM $SrCl_2$ and solution No. 8 is composed of 0.395 M NH_4Cl, 148.42 mM $CaCl_2$ and 1.5 mM $SrCl_2$. NH_4Cl is used here to buffer the solution and to adjust the ionic strength of the solutions. All the chemicals are ACS grade of Merck and all solutions were prepared using deionized water (18.2 MΩ).

In this technique 400–550 ml of NH_4Cl-$CaCl_2$-$SrCl_2$-solution and the solid $(NH_4)_2CO_3$ (ammonium carbonate) are contained within a sealed reacting chamber as it is described in AlKhatib and Eisenhauer (2017). In all experiments the reacting solution is stirred with a magnetic stirrer at 300 rounds per minute. Ammonium carbonate decomposes spontaneously and produces an ammonia/carbon dioxide atmosphere within the chamber by the reaction:

$$(NH_4)_2CO_{3(s)} \leftrightarrow 2NH_{3(g)} + CO_{2(g)} + H_2O_{(g)} \quad (1)$$

Ammonia and carbon dioxide gases diffuse and dissolve in the experimental solution increasing pH and alkalinity by the following reactions

$$NH_{3(g)} + H_2O \leftrightarrow NH^+_{4(aq)} + OH^-_{(aq)} \quad (2)$$

$$CO_{2(g)} + H_2O \leftrightarrow CO_{2(aq)} \quad (3)$$

$$CO_{2(aq)} + H_2O \leftrightarrow H_2CO_3 \quad (4)$$

$$H_2CO_3 \leftrightarrow HCO^-_{3(aq)} + H^+_{(aq)} \quad (5)$$

$$HCO^-_{3(aq)} \leftrightarrow CO^-_{3(aq)} + H^+_{(aq)} \quad (6)$$

The overall spontaneous reaction of the steps (1)–(6) is:

$$(NH_4)_2CO_3(s) \rightarrow 2NH^+_4(aq) + CO^{2-}_3(aq)$$

The result of these reactions is the supersaturation of the reacting solution with respect to aragonite. The dynamic of the reaction was monitored by a WTW 3100 pH meter which was standardized against a buffer solutions of pH 4, 7 and 10 before each single experiment. This pH meter connected to a computer monitors the pH values and the

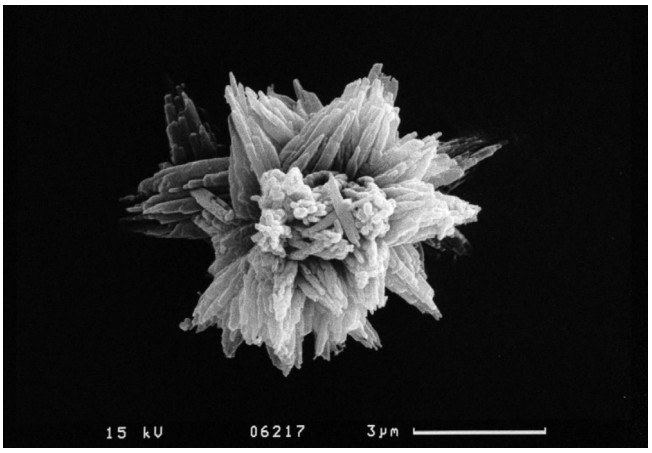

Fig. 1. SEM images of a typical aragonite aggregate (arbitrarily selected from experiment 35B). The needle like structure of an aragonite crystal can well be distinguished from the hexagonal structure of a calcite crystal.

temperature of the solution online (see Fig. 1 in AlKhatib and Eisenhauer (2017)) continuously and stores the measured data in an excel sheet. We controlled the rate of reaction as well as the time needed to reach the precipitation point by the quantity, the surface area of the granules of ammonium carbonate and by the membrane porosity through which the gases diffuse. For example for slow reaction rates we use 5–10 g of ammonium carbonate with a radius of about one centimeter. To accelerate the reactions we put an additional beaker containing solid ammonium carbonate (different quantities and different particle size) inside the reacting chamber. This beaker was covered with parafilm of distinct porosity. In certain cases the beaker was not covered at all, then the rate of reaction increased rapidly. The time needed to start precipitation ranged between 24.7 and 3.2 h depending on the temperature of the individual reaction.

During the experiment the chemical evolution of the reacting solution was monitored by sampling 2–5 ml at distinct time intervals ranging between 5 and 30 min depending on the reaction time to be analyzed later. We allowed each reaction to run for a certain period of time depending on its rate then stopped it by removing the reacting solution from the sealed chamber and filter the solution as fast as possible by vacuum filtration through a cellulose filter paper with a pore size of 0.2 µm. Then the solid was washed with deionized water (18.2 MΩ) and mixed with a small volume of pure ammonium hydroxide solution to make it slightly alkaline. Furthermore, the filter was finally washed with pure ethanol in order to remove any adsorbed $CaCl_2$ or/and $SrCl_2$ aqueous solutions on the surface of the crystals.

2.1.1. Mineralogy of the precipitates

In order to demonstrate the precipitation of aragonite by our experimental setup we added two arbitrarily selected XRD spectra to the appendix. From Fig. A1 it can clearly be seen that the precipitated material shows the typical characteristic peaks for aragonite. In addition the SEM picture of arbitrarily selected sample of experiment 35B (Fig. 1) shows the typical orthohombric structure and needle like structure of an aragonite crystal (Gutjahr et al., 1996). Latter structure can be well distinguished from a calcite crystal showing a hexagonal surface structure (Alkhatib and Eisenhauer, 2017). Furthermore, the trace element composition e.g. Sr/Ca distribution in our calcite samples is ~0.1 in calcite and ~1 in the samples we consider here to be aragonite (Kinsman and Holland, 1969). In addition the measured Mg absorption coefficient (D_{Mg}) values as measured in our aragonite samples are in the order of $5 \cdot 10^{-4}$ to about $1.6 \cdot 10^{-3}$ in accordance with typical values published elsewhere in the literature (c.f. Kisakürek et al., 2008; Wombacher et al., 2011). Note we are defining D_{Mg} as an adsorption rather than a partitioning coefficient because of its low abundance in aragonite. Magnesium may not become incorporated rather only adsorbed on its surface.

In summary, there is plenty of evidence that the material precipitated throughout the experiments described above produced aragonite rather than calcite and high Mg-calcite, respectively. Note, that all solutions are supersaturated with respect to strontianite ($SrCO_3$, Table 4, column 8). Although it cannot be identified from the XRD spectra (see Appendix A, Fig. A1) the abundance of $SrCO_3$ in our aragonite samples cannot completely excluded due to analytical resolution problems related to the conventional XRD techniques (Greegor et al., 1997).

2.2. Analysis

2.2.1. Dissolved in organic carbon (DIC)

The details to determine [DIC] in our system has been described earlier in Alkhatib and Eisenhauer (2017). In brief to calculate DIC, the total alkalinity (TA) of each experiment through the whole period of reaction has to be calculated. We did this by titrating 0.2 ml of the reaction mixture at different intervals of time during the precipitation reaction against 0.02 N HCl (dilution of MERCK-Titrisol-solution™). This HCl solution is initially standardized against IAPSO seawater (Certified alkalinity of 2.325 mM) using a micro titration apparatus Metrohm 665 Dosimat equipped with a titration vessel of 7 cm. During the titration the sample is degassed with nitrogen

continuously to remove any CO_2. The indicator used in this titration is prepared from two solutions. Solution 1: about 1–32 mg Methyl Red (or 37 mg of sodium salt of Methyl Red) mixed with 1.19 ml of 0.1 M NaOH and dissolved in 80 ml 96% ethanol. Solution 2: about 2–10 mg Methylene Blue dissolved in 10 ml 96% ethanol. Taking 4.8 ml of solution 2 and mixing it with 80 ml of solution 1 to obtain a greenish-brown solution, at the end point of the titration solution becomes pink. In each titration the indicator volume used was 20 µl added to 4.8 ml of water and 0.2 ml sample. Each sample was titrated three times and the average volume was used to calculate the total alkalinity.

Furthermore the concentration of ammonia $[NH_3]_{aq}$ in our samples has to be determined and the apparent acid dissociation constant of ammonium chloride in our experimental condition has to be calculated ($K_a = [NH_3]\,[H^+]/[NH_4^+]$; K_a = dissociation constant). The value for K_a had to be determined because only one value for 20 °C was known before (Lemarchand et al., 2004). Following this 6 ml aliquot of the mother solution was titrated potentiometrically against 1 M $[NaOH]_{aq}$ using the micro titration apparatuses. The average volume of the three titration trials was 2.40 ml NaOH. Then the pH of half neutralized mother solution was measured in a thermostat at different temperatures. At each temperature the half neutralized solution was kept at least 30 min in the thermostat in order to reach thermal equilibrium before measuring its pH. The salinity of the reaction mixtures was measured by WTW cond. 3110 set 1.

2.2.2. Elemental analysis

Elemental analyses have been performed in the same way as described in Alkhatib and Eisenhauer (2017). In order to calculate the precipitation rate of each single reaction for Sr and Mg incorporation into aragonite, we analyzed the concentrations of [Ca], [Mg] and [Sr] ions in the mother solutions at different intervals of time during the course of each reaction. Furthermore, the final solution of each individual reaction as well as the elemental ratio in the precipitates was measured by inductively coupled plasma mass spectrometry (ICP-MS; Agilent Technologies 7500 Series). The initial concentration of Mg^{2+} in all samples was set to be 30 mM except in samples 9 and 10 were it was set to 150 and 60 mM, respectively. In the final solutions $[Mg^{2+}]$ is very close to the initial solutions and the decrease in concentration is within the uncertainty of the initial concentration. For quality control and accuracy Indium (In) as an internal standard was used in combination with a multi standard calibration method (Ca, Mg and Sr in 2% HNO_3-ultra pure distilled HNO_3). Each sample was analyzed at least three times. For analyzing solid products all samples were diluted in 2% HNO_3 to reach 25.0 ± 2.5 ppm Ca in order to avoid matrix effects. Coral standard JCP-1 was used as a reference material and measured as every fifth sample and in a total of thirty-one times during the course of this study ($N = 31$). The JCP-1 Sr/Ca and Mg/Ca ratios were calculated to be 8.80 ± 0.06 and 4.18 ± 0.03 mmol/mol respectively, which match within the statistical uncertainty the reported values of 8.84 $\pm$ 0.09 Sr/Ca and 4.2 ± 0.1 Mg/Ca mmol/mol of Hathorne et al. (2013). The average uncertainty for our Sr/Ca ratios is 0.04 mmol/mol and for Mg/Ca it is 0.02 mmol/mol corresponding to the 95% confidence level.

2.2.3. Crystalline structure and specific surface area of aragonite products

Similar as reported in AlKhatib and Eisenhauer (2017) the crystalline structure of the solid products were analyzed at the Geology Department of Kiel University by X-ray diffraction and by scanning electron microscope (SEM) CamScan-CS-44, equipped with a secondary electron detector, backscattered electron detector, thermal evaporator Edwards Auto 306 and sputtering-coater EMITECH K550, Au/Pd (80/20). Measurements were performed with an X-ray-diffractometer "D8 Discover" (Bruker AXS). The samples were analyzed in a 2Θ-range from 4° to 90° with a step size of 0.007° and counting time 1.5 s/step using a Cu X-ray radiation source. Software for data evaluation (High Score Plus Version 3.0d (3.0.4)) is provided by PANalytical. Specific surface area of the final aragonite products was determined applying the Brunauer-Emmett-Teller (BET) gas adsorption method (De Kanel and Morse, 1979). Of the total number of 35 aragonite samples produced in this study we analyzed 23 having enough material (60 mg) to become analyzed by the BET method. Measurements were carried out at the institute of Geology, Mineralogy and Geophysics, Ruhr University Bochum, Germany.

For later comparison of precipitation rates (R^*) for calcite (AlKhatib and Eisenhauer, 2017) and aragonite (this study) we note that R^* values for calcite have been determined via SEM measurements in contrast to the applied BET method in this study. A change of the method for the determination of the specific surface area for aragonite was necessary because in contrast to calcite the aragonite crystal show a rhombohedral needle like structure of irregular shape. This makes it impossible quantifying single crystal surfaces by SEM. Rather the BET method had to be applied (De Kanel and Morse, 1979). In order to verify comparability we also determined the specific surface area of a commercial calcite (Roth, $CaCO_3 > 99\%$, Art.-Nr. P012.2) by both BET and SEM, respectively. As a result both methods independently gave the same value of ~ 0.5 m^2/g within an uncertainty of 15%. Latter agreement indicates that no significant corrections for the specific surface methods as a function of the method is necessary and that the calculated precipitation rates of aragonite and calcite are comparable within their uncertainty in this study.

2.2.4. Strontium and calcium isotope analysis

Isotope measurements for Ca and Sr isotopes were carried out at the GEOMAR mass spectrometer facilities in Kiel, Germany, with a ThermoFisher Triton T1 Thermal-Ionization-Mass-Spectrometer (TIMS) as it is described in AlKhatib and Eisenhauer (2017).

At least two isotope measurements (ic-run and id-run) have to be performed for a single Sr isotope measurement. One unspiked run (ic-run, isotope composition) and one run with an $^{87}Sr/^{84}Sr$-double spike added to the sample solution (id-run, isotope dilution). Sample size was selected

to be in the order of 1500 ng of Sr. Spike correction and normalization of the results was carried out as earlier described by Krabbenhöft et al. (2009). For quality control the following standard materials were applied: SRM987 $SrCO_3$ standard from the National institute of standards and technology (NIST), JCp-1 coral standard and IAPSO seawater standard. We report the statistical uncertainties of our measurements as twice the standard deviation of the mean (SE = standard error, $2\sigma_{mean} = 2\sigma/n^{0.5}$); where n is the number of measurements per value. The measured $^{88}Sr/^{86}Sr$ ratios are reported in the common δ-notation relative to NIST SRM987: $\delta^{88/86}Sr\ (‰) = [(^{88}Sr/^{86}Sr)_{sample}/(^{88}Sr/^{86}Sr)_{SRM987} - 1]$. The blank values of our chromatographic column separations were <0.10 ng Sr as a whole procedure blank in all batches we prepared. The $\delta^{88/86}Sr$-values of column separated SRM987 chemistry was measured in three different batches and has these values (0.00 ± 0.02, 0.018 ± 0.014 and $0.003 \pm 0.005‰$, $n = 4$ for each) showing insignificant deviations from the reference values due to the column separation of the standard. The $\delta^{88/86}Sr$-values of separated IAPSO of our three batches resulted into (0.372 ± 0.006, 0.399 ± 0.001 and $0.392 \pm 0.005‰$, $n = 4$ for each) which compares well with the long term IAPSO average of the instrument measurements of $0.391 \pm 0.004‰$, $n = 63$. The $\delta^{88/86}Sr$-values of separated JCP-1 of our three batches are: 0.188 ± 0.006, 0.200 ± 0.010 and $0.196 \pm 0.004‰$, $n = 4$ for each). Latter values are in agreement with the mean value carried out by this instrument of ($0.195 \pm 0.003‰$, $n = 87$).

The method adopted for Ca isotope measurement follows Heuser et al. (2002) and Böhm et al. (2006), respectively. For each sample to be analyzed 3000 ng of Ca were spiked with 120 µl $^{43}Ca/^{48}Ca$ double spike to correct for isotope fractionation in the mass spectrometer during the course of the Ca isotope analysis. The mixture was evaporated to dryness and then redissolved in 100 µl 0.9 N HCl. This solution was loaded onto an ion exchange column (BIO RAD of 800 µl volume; cation exchange resin MCI Gel, CK08P, 75–150 µ, Mitsubishi chemical composition) in order to extract the Ca-fraction. After washing the column with water (18.2 MΩ) and then with 1.5 N HCl, sample was then loaded to the column, washed with 3.5 ml 1.5 N HCl. The Ca-fraction was then eluted after rinsing the column with 9 ml 1.5 N HCl. Then the solution was evaporated to dryness and redissolved in 20 µl 2.5 N HCl. This quantity is enough to load ten filaments to measure ten separate runs. Details of the measurement procedure can be found in Heuser et al. (2002) and Böhm et al. (2006). In each run session NIST SRM915a was measured four times, CaF_2 was measured twice (which used as a control standard) and each sample was measured at least five times. The isotopic ratio of each sample as well as CaF_2 was normalized to the mean of the four $^{44}Ca/^{40}Ca$ NIST SRM915a analysis during the course of this study and reported in the common delta notation $\delta^{44/40}Ca\ (‰) = [(^{44}Ca/^{40}Ca)_{sample}/(^{44}Ca/^{40}Ca)_{standard} - 1]$. The blank values of our chromatographic column separations were <15 ng of Ca as a whole procedure blank in all batches we prepared. The average of $\delta^{44/40}Ca$ values of separated NIST SRM915a by column chemistry was measured 12 times in three different batches resulted in $0.02 \pm 0.02‰$ showing insignificant deviation due to the column separation of the standard. The average of the $\delta^{44/40}Ca$ values of our CaF_2 standard measured in 20 different runs was $1.4 \pm 0.2‰$ ($n = 40$) which is in absolute agreement with earlier measurements (c.f. Heuser et al., 2005).

For discussion we are reporting Sr and Ca fractionation in the big delta notations $\Delta^{88/86}Sr_{aragonite\text{-}aq} = \delta^{88/86}Sr_{aragonite} - \delta^{88/86}Sr_{aq}$ and $\Delta^{44/40}Ca_{aragonite\text{-}aq} = \delta^{44/40}Ca_{aragonite} - \delta^{44/40}Ca$ (aq = initial solution), respectively. All Δ-values are corrected for the reservoir or Rayleigh distillation effect (Zeebe and Wolf-Gladrow, 2001). In brief a correction for the "reservoir effect" is considered when the reservoir (bulk solution) is not infinite rather than relatively small compared to the amount of solid material precipitating out of this reservoir (Böhm et al., 2012; Fruchter et al., 2016). Given a kinetic isotope fractionation where the light isotopes are enriched in the solid the reservoir becomes enriched in the heavy isotope. Latter effect is small to negligible when the reservoir is infinite and the amount of precipitated material is relatively small. However, is the amount of material in the reservoir comparable to the amount of precipitated material latter value deviate from an infinite reservoir as a function of the relative amount precipitated from solution. The isotope values measured in the solid precipitated from a restricted reservoir would then tend to show higher values to those values precipitated from an infinite reservoir. In our case the reservoir correction is actually quite small or negligible for Sr (Fig. A2) because only a small fraction of Sr co-precipitated with Ca. In this regard for Sr the reservoir can be considered to be infinite. In contrast corrections are larger for Ca because a significant amount of up to 90% of all dissolved Ca precipitated out of solution. Correction for the reservoir effect (Table 4) leads to an increase of the measured values of up to a maximum of ~0.5‰, respectively. For more quantitative information we refer to the appendix of AlKhatib and Eisenhauer (2017).

3. RESULTS

In the following section the determination of those parameters important for the calculation of the aragonite precipitation rates (R (mmol/h), R^* (mmol/(m^2·h))) are described and applied to our data. Note, that the concentrations of NH_3 and NH_4 in our experimental setup are about one order of magnitude higher when compared with the concentrations for example used in Tang et al. (2008). Latter fact inhibits the calculations of activity coefficients applying geochemical modeling and the PHREEQC software. Consequently, all calculations are based on concentrations only.

3.1. pH, TA, NH_3, DIC, metal ion concentrations and saturation indexes with respect to different forms of $CaCO_3$ and with respect to $SrCO_3$

For the calculation of precipitation rates (R^*) the quantitative knowledge of pH, [TA], [NH_3] and [DIC] is important. In particular [NH_3] is important to know in order to

determine [TA], [HCO_3^-] and [CO_2^{2-}]. Throughout the reaction the pH of the reacting solution (when precipitation starts) remains relatively constant (±0.02 units) as well as the temperature of all reactions (±0.2 °C). During the course of the experiment we determined [TA] by online measurement and verified that [TA] of the precipitation solutions is kept constant within ±10% throughout time. Concentrations of [NH_3], [HCO_3^-] and [CO_3^{2-}] were calculated as shown in AlKhatib and Eisenhauer (2017). Details on carbonate speciation, [DIC] as well as the metal ion concentrations in the initial and final solutions are summarized in Table 1. For details of calculations of the chemical kinetic we refer to AlKhatib and Eisenhauer (2017) and the appendix therein. Saturation state (Ω) is calculated following Millero (1995):

$$\Omega = [Me^{2+}][CO_3^{2-}]/k_{sp}, \text{saturation index (SI)} = \log\Omega, \quad (7)$$

where Me^{2+} is either Sr^{2+} or Ca^{2+} and k_{sp} is the solubility product constant of the solid product. Values of k_{sp} of aragonite, amorphous $CaCO_3$ (ACC) and $SrCO_3$ are shown in Table 2. It can be seen from Table 4 that all sample reactions are oversaturated with respect to aragonite, ACC and $SrCO_3$.

3.2. Kinetics of aragonite formation reactions

3.2.1. Initial rate of reaction (R) and the order of reaction with respect to Ca and bicarbonate ions

In order to determine the precipitation rate R we applied the "initial rate method" because of the closed system character of the experiment and because of its simplicity. In the appendix details on the application of the initial rate method to calculate R and the order of reaction "x" for Ca and "y" for DIC and HCO_3^-, respectively, is explained in more detail applying it to arbitrarily selected sample 34F (see Appendix A).

The problem determining R is that depending on the experimental conditions and a possible non-linear behavior chemical equilibrium has to finally reached in order to calculate an average precipitation rate. However, the experimental experience shows that the precipitation of $CaCO_3$ is relatively fast, quantitative and linear in the beginning of the precipitation. Hence, the approximation of the linear part of this reaction by a linear fit of the first data points is a good measure of the average precipitation rate for the whole precipitation process until equilibrium is reached. Applying this to all experiments we exclude the problem of reaching the chemical equilibrium and make all values more comparable. A further advantage is that neither assumption has to be made nor constants have to be known in advance and the method is straight forward. That the linear rate method is a good approximation for the whole precipitation process is also supported by the finding that in between 33 and ~100% of the $CaCO_3$ precipitated linearly shortly after precipitation started.

3.2.2. Calculation of aragonite activation energy

From an approximation of our three calculated rate constants (Table 3) at 12.5, 25 and 37.5 °C we fit the Arrhenius equation:

$$\ln k = -\frac{E_a}{RT} + \ln A, \; k \text{ is the rate constant } (\mathrm{mM}^{-x}\,\mathrm{h}^{-1}), \quad (8)$$

where "x" is the order of reaction with respect to HCO_3^- ions E_a = activation energy, R = gas constant (8.314 J/° K mol)) and T(K) is the temperature, A ("frequency factor") is a constant which corresponds to the intercept of the line at $1/T \sim 0$ (at infinite temperature).

From the slope calculated to be ~−17,881 we can estimate E_a for the aragonite formation to be ~149 kJ/mol about ~35 kJ/mol (114 kJ/mol for calcite, AlKhatib and Eisenhauer, 2017) higher than the one for calcite. Latter value for aragonite is in general agreement with the expectation to have E_a for aragonite to be higher than the one for calcite. The comparison with literature data as reported by Romanek et al. (2011) who estimated E_a of inorganic precipitated aragonite using a seeded-growth technique, in absence of both ammonia and ammonium to be 71.2 kJ/-mole. Probably, latter slight discrepancy between the data is attributed to different experimental setups and the use of seed crystals.

The knowledge of E_a is important to identify the rate limiting step because when E_a is higher than 50 kJ/mole, precipitation mechanism is too a large extend surface or chemical-controlled and not diffusion-controlled (Gutjahr et al., 1996; Petrou and Terzidaki, 2014). This means that transport of material to the mineral surface from the bulk solution through a distinct boundary layer is still occurring but no longer the only rate determining step. Rather processes at the solid surface might become the rate determining step, which includes adsorption of reactive solutes to the surface itself, surface diffusion, bond formation or cleavage, ionic exchange with the solid and loss of solvent water (Morse et al., 2007).

3.2.3. Crystalline structure and precipitation rate normalized to the surface area

X-ray diffraction showed that 100% of all solid products are pure aragonite without detecting any amount of $SrCO_3$ in any of the solid samples even though all samples are oversaturated with respect to $SrCO_3$ (Table 4). However, the presence of $SrCO_3$ in the samples cannot be completely ruled out because it may not be visible in the XRD spectra due to analytical resolution issues. The issue of $SrCO_3$ co-precipitation is yet not solved and may be quite complex possibly interfering with Sr isotope fractionation also. Further experiments have to quantify this influence. Concerning the study here SEM images showed that aragonites precipitated similar under different experimental conditions having needle like crystalline structures all the time as shown in Fig. 1.

From Fig. 2 it can be seen that the specific surface areas (S) of aragonite products are independent of temperature and R. Hence it can be assumed that S of all aragonite products are equal to the average value 2.7 ± 0.4 m^2/g or equivalent to 270 ± 20 m^2/mole (± is $2\sigma_{mean}$). From this value the normalized rate of reaction R^* (μmol/m^2 h) is calculated by dividing R of each reaction by S and the corre-

Table 1
Temperature (T), total alkalinity (TA), pH, salinity, concentration of ammonia [NH_3], dissolved inorganic carbon [DIC], mole fraction of bicarbonate in [DIC], initial and final concentrations of both [Ca] and [Sr] and their remaining fraction at the end of each experiment, Sr/Ca and Mg/Ca in aragonite, the ratio of initial $[Ca]_0$ to the concentration of the dissolved inorganic carbon (Ca_0:DIC), Sr:Ca ratio in the mother solution ($[Sr]_0/[Ca]_0$), volume of aqueous solution, moles of $CaCO_3$ produced and its surface area.

Sample label	$T \pm 0.2$ (°C)	TA (mM)	pH	Salinity	$[NH_3]$ (mM)	[DIC] (mM)	$[CO_3]$ (mM)	$[HCO_3]$ (mM)	Mole fraction of $[HCO_3]$ in [DIC]	$[Ca]_0$ (mM)	$[Ca]_f$ (mM)	Fraction of Ca remaining	$[Sr]_0$ (mM)	$[Sr]_f$ (mM)	Fraction of Sr remaining	Sr/Ca (mmol/mol)	Mg/Ca (mmol/mol)	$[Ca]_0$ [DCI]	$[Sr]_0/[Ca]_0$	Volume of solution (ml)	Moles of $CaCO_3$	Area of $CaCO_3$ (m^2)
1	**2**	**3**	**4**	**5**	**6**	**7**	**8**	**9**	**10**	**11**	**12**	**13**	**14**	**15**	**16**	**17**	**18**	**19**	**20**	**21**	**22**	**23**
50C	37.5	57.93	8.629	34.7	42.05	15.88	4.97	5.94	0.54	10.22	3.03	0.30	0.100	0.029	0.29	9.94	4.14	0.64	0.010	400	0.00288	0.768
50D	37.5	74.83	8.722	35.0	52.86	21.97	7.41	7.15	0.49	10.11	2.13	0.21	0.049	0.010	0.20	5.06	5.30	0.46	0.005	400	0.00319	0.852
51E	37.5	27.35	8.230	35.2	16.57	10.78	2.16	6.47	0.75	10.33	4.86	0.47	0.101	0.046	0.46	10.06	2.67	0.96	0.010	400	0.00219	0.584
51F	37.5	30.67	8.293	35.5	19.19	11.49	2.50	6.48	0.72	10.16	4.30	0.42	0.049	0.020	0.41	4.96	2.83	0.88	0.005	400	0.00234	0.626
52G	37.5	32.63	8.344	35.1	21.56	11.07	2.57	5.93	0.70	10.61	5.81	0.55	0.051	0.027	0.53	4.91	2.58	0.96	0.005	400	0.00192	0.513
52H	37.5	31.36	8.327	35.1	20.71	10.65	2.42	5.80	0.71	10.13	6.59	0.65	0.099	0.064	0.65	10.02	2.37	0.95	0.010	400	0.00142	0.378
24A	37.5	21.98	8.130	38.2	13.10	8.88	1.54	5.80	0.79	11.16	5.30	0.47	0.110	0.052	0.47	9.92	2.16	1.26	0.010	550	0.00322	0.861
24 B	37.5	19.05	8.080	38.8	11.63	7.42	1.19	5.04	0.81	11.19	5.79	0.52	0.056	0.029	0.52	4.80	2.15	1.51	0.005	550	0.00297	0.793
25D	37.5	45.23	8.452	35.6	28.06	17.17	4.52	8.12	0.64	10.50	2.42	0.23	0.052	0.012	0.23	4.98	5.08	0.61	0.005	550	0.00445	1.187
26E	37.5	32.53	8.300	35.4	19.57	12.96	2.85	7.26	0.72	10.42	2.59	0.25	0.103	0.025	0.24	9.74	2.76	0.80	0.010	550	0.00431	1.151
26F	37.5	28.13	8.235	35.8	16.78	11.35	2.29	6.77	0.75	10.39	3.65	0.35	0.052	0.018	0.35	4.89	3.55	0.92	0.005	550	0.00371	0.990
27H	37.5	29.01	8.242	35.7	17.08	11.93	2.43	7.07	0.74	10.32	3.52	0.34	0.103	0.034	0.33	9.84	3.27	0.87	0.010	550	0.00374	0.998
28A	25.0	21.49	8.156	36.3	13.80	7.69	1.00	5.70	0.85	10.73	7.58	0.71	0.109	0.071	0.65	10.51	1.91	1.40	0.010	550	0.00174	0.464
28B	25.0	21.59	8.160	36.4	13.93	7.66	1.00	5.66	0.85	10.39	6.88	0.66	0.053	0.033	0.62	5.62	1.65	1.36	0.005	550	0.00193	0.515
29C	25.0	27.26	8.223	35.0	16.24	11.02	1.60	7.82	0.83	10.31	4.25	0.41	0.105	0.038	0.37	10.32	3.49	0.94	0.010	550	0.00333	0.890
29D	25.0	21.69	8.116	35.2	12.63	9.06	1.10	6.86	0.86	10.11	4.85	0.48	0.051	0.022	0.43	5.33	2.63	1.12	0.005	550	0.0029	0.773
30E	25.0	19.15	7.944	35.3	8.53	10.61	0.94	8.74	0.90	10.12	4.53	0.45	0.103	0.040	0.39	10.44	3.14	0.95	0.010	550	0.00307	0.820
30F	25.0	20.32	8.029	35.2	10.36	9.96	1.03	7.90	0.88	10.34	4.23	0.41	0.051	0.019	0.37	5.40	3.17	1.04	0.005	550	0.00336	0.897
31A	25.0	45.62	8.370	35.3	23.41	22.21	4.05	14.12	0.78	10.05	1.49	0.15	0.103	0.012	0.11	10.54	5.90	0.45	0.010	550	0.00471	1.256
31B	25.0	40.15	8.348	35.2	22.03	18.12	3.19	11.73	0.79	10.09	1.63	0.16	0.052	0.006	0.12	5.35	4.35	0.56	0.005	550	0.00465	1.241
49A	25.0	35.27	8.386	34.6	23.67	11.60	2.16	7.27	0.77	10.11	4.33	0.43	0.049	0.020	0.40	5.28	4.83	0.87	0.005	400	0.00231	0.617
49B	25.0	39.86	8.438	34.5	26.78	13.08	2.62	7.83	0.75	10.17	4.18	0.41	0.049	0.019	0.38	5.18	5.79	0.78	0.005	400	0.0024	0.640
9	25.0	15.20	7.820	79.0	7.90	7.30	0.55	6.20	0.92	142.77	132.39	0.93	1.550	1.411	0.91	12.41	3.88	19.56	0.011	400	0.00415	1.109
10	25.0	22.30	8.069	40.0	12.10	10.20	1.05	8.10	0.89	18.54	9.77	0.53	0.236	0.111	0.47	12.50	6.20	1.82	0.013	400	0.00351	0.936
11	25.0	21.67	8.113	35.0	13.37	8.30	0.87	6.57	0.88	8.96	2.82	0.31	0.120	0.032	0.26	12.60	3.34	1.08	0.013	400	0.00246	0.656
32A	12.5	12.89	7.791	36.2	5.95	6.95	0.29	6.37	0.96	10.49	5.44	0.52	0.104	0.048	0.46	12.22	1.44	1.51	0.010	550	0.00278	0.741
32B	12.5	15.63	7.850	36.4	6.84	8.79	0.41	7.96	0.95	10.40	7.16	0.69	0.052	0.034	0.65	6.11	2.28	1.18	0.005	550	0.00178	0.475
33C	12.5	17.68	8.028	35.1	10.27	7.41	0.50	6.40	0.93	10.39	7.33	0.71	0.104	0.072	0.69	12.14	2.23	1.40	0.010	550	0.00168	0.449
33D	12.5	16.61	8.004	35.0	9.71	6.90	0.45	6.01	0.93	10.18	6.86	0.67	0.051	0.032	0.63	6.11	2.36	1.48	0.005	550	0.00183	0.488
34E	12.5	20.71	8.029	35.0	10.37	10.34	0.70	8.93	0.93	10.31	4.39	0.43	0.102	0.038	0.37	11.42	3.83	1.00	0.010	550	0.00326	0.870
34F	12.5	22.18	8.000	35.3	9.75	12.42	0.80	10.83	0.93	10.26	3.53	0.34	0.050	0.014	0.28	5.73	3.86	0.83	0.005	550	0.00371	0.989
35A	12.5	16.51	7.962	35.0	8.83	7.68	0.46	6.77	0.94	9.89	6.58	0.67	0.101	0.062	0.61	11.61	4.31	1.29	0.010	550	0.00182	0.486
35B	12.5	18.27	8.002	35.3	9.70	8.56	0.55	7.46	0.93	9.75	5.06	0.52	0.050	0.022	0.44	5.84	3.91	1.14	0.005	550	0.00258	0.688
36C	12.5	21.10	8.071	35.2	11.41	9.70	0.72	8.26	0.92	9.76	5.42	0.56	0.100	0.050	0.50	11.41	5.96	1.01	0.010	400	0.00174	0.464
36D	12.5	26.47	8.167	35.3	14.31	12.16	1.08	10.00	0.90	9.77	3.82	0.39	0.050	0.016	0.32	5.58	6.88	0.80	0.005	400	0.00238	0.636

Notes: TA was measured from titrating the final solution with HCl. The pH and salinity were measured at the end of each reaction. $[NH_3]$, $[CO_3^{2-}]$, [DIC] and $[HCO_3^-]$ were calculated as in Lemarchand et al. (2004) and AlKhatib and Eisenhauer (2017). Mole fraction of HCO_3^- column 10 = (column 9)/(column 9 + column 8). Initial and final [Ca] and [Sr] (columns 11–18) are measured by ICP-MS. Column 13 = column 12/column 11. Column 16 = column 15/column 14. Column 19 = column 11/column 7. Column 20 = column 14/column 11. Column 22 = [(column 11 − column 12) * column 21] * 10^{-6}. Column 23 = column 22 × 267 m^2/mol.

Table 2
K_{sp} of aragonite, ACC and strontianite.

T/°C	K_{sp}-aragonite (10^7)	K_{sp}-ACC (10^7)	K_{sp}-$SrCO_3$ (10^{10})
37.5	6.13	6.17	4.98
25.0	6.60	9.09	5.36
12.5	6.87	13.85	5.24

Notes: K_{sp}-aragonite calculated as in Millero (1995) at salinity (S) = 35.5 except for samples 9 and 10 $K_{sp} = 35.60 \cdot 10^{-7}$ and $7.71 \cdot 10^{-7}$ respectively, K_{sp}-ACC as in Clarkson et al. (1992) and K_{sp}-$SrCO_3$ as in Busenberg et al. (1984).

Table 3
Order of reactions with respect to HCO_3^- ions and the rate constant at three different temperatures.

T (°C)	Order of reaction with respect to DIC	Rate constant $mM^{-x}\ h^{-1}$
1	**2**	**3**
12.5	3	$1.01 \cdot 10^{-4}$
25.0	2	$17.32 \cdot 10^{-4}$
37.5	1	$154.67 \cdot 10^{-4}$

Note: Values of this table are obtained by treating data as described in (AlKhatib and Eisenhauer submitted) Section 3.2.2.

sponding individual sample weight (see also AlKhatib and Eisenhauer, 2017).

$$R^* = [\text{initial rate (mM/h)} \times \text{volume of solution (ml)}]/S\ (m^2/g) \times \text{Sample weight (g)} \quad (9)$$

Note that the specific surface area of aragonite (270 ± 20 m^2/mole) is a factor of 4.5 larger than the one of calcite estimated to be 59 m^2/mol AlKhatib and Eisenhauer (2017).

3.3. Strontium and magnesium incorporation into aragonite

Incorporation of Sr and Mg can be calculated among other approaches described by the equation of Holland et al. (1963) and Usdowski (1975) where D_{Sr} is the the distribution coefficients of Sr ($([Sr]/[Ca])_{aragonite}/([Sr]/[Ca])_{aq}$) in aragonite. Following (Usdowski, 1975) we get:

$$([Sr]/[Ca])_{aragonite} = ([Sr]/[Ca])_{aq,0} \times \left\{1 - ([Ca]/[Ca]_0)^{DSr}\right\} \Big/ \left\{1 - ([Ca]/[Ca]_0)_{aq}\right\}. \quad (10)$$

where $([Sr]/[Ca])_{aragonite}$ is the molar ratio of the aragonite, $([Sr]/[Ca])_{aq,0}$ is the molar ratio of these ions in the solution, $([Ca]/[Ca]_0$ is the fraction of Ca that remains in aqueous solution at any time and D_{Sr} is the distribution constant of Sr between solution and the aragonite ($D_{Sr} = [Sr]/[Ca])_{aragonite}/[Sr]/[Ca])_{aq}$).

Concerning Mg we define an adsorption rather than a distribution coefficient due to the fact that Mg is rather adsorbed than incorporated. However, concerning the definition there is no difference in the expression. Following this approach the adsorption coefficient (D_{Mg}) of Mg is defined as $([Mg]/[Ca])_{aragonite}/([Mg]/[Ca])_{aq}$ in aragonite similar to the definition for Sr.

From Fig. 3 it can be seen that most of the D_{Sr} values are above zero indicating that relative more Sr is taken up from the solution when compared to the initial $([Sr]/[Ca])_{aq,0}$ ratio. At 12.5 °C as R^* increases D_{Sr} values decrease without any dependency on the initial $([Sr]/[Ca]_{0,aq})$-ratio in the reacting solution. However at 25.0 °C a discrepant behavior of D_{Sr} values can be observed. At a $([Sr]/[Ca]_{0,aq})$ initial ratio of 0.01 D_{Sr} values tend to increase as a function of R^*. In contrast when the initial $([Sr]/[Ca]_{0,aq})$ ratio is 0.005 mmol/mol D_{Sr} values tend to decrease as a function of R^*. At 37.5 °C as R^* increases D_{Sr} values increase without any significant effect of the initial $([Sr]/[Ca]_{0,aq})$ ratio. The temperature effect on the D_{Sr} values is much more significant than the rate effect itself. The R^*–D_{Sr} relationships are:

$$\mathbf{37.5\ ^\circ C}: \log D_{Sr} = 0.03 \pm 0.01 \log R^* - 0.10 \pm 0.04,\quad R^2 = 0.80,\quad P = 9.40E-05 \quad (11)$$

$$\mathbf{25.0\ ^\circ C\ and\ [Sr]/[Ca]_o = 0.01} \quad (12)$$

$$\log D_{Sr} = 0.04 \pm 0.04 \log R^* - 0.08 \pm 0.14,\quad R^2 = 0.53,\quad P = 0.065$$

$$\mathbf{25.0\ ^\circ C\ and\ [Sr]/[Ca]_o = 0.005} \quad (13)$$

$$\log D_{Sr} = -0.02 \pm 0.02 \log R^* + 0.11 \pm 0.08,\quad R^2 = 0.53,\quad P = 0.1$$

$$\mathbf{12.5\ ^\circ C}: \log D_{Sr} = -0.03 \pm 0.02 \log R^* + 0.17 \pm 0.05,\quad R^2 = 0.69,\quad P = 0.0028 \quad (14)$$

From Fig. 4 it can be seen that D_{Mg} values increase with increasing R^* but decreases as temperature increase. The dependency on R^* can be determined as follows:

$$\mathbf{37.5\ ^\circ C}: \log D_{Mg} = 0.16 \pm 0.22 \log R^* - 3.73 \pm 0.76,\quad R^2 = 0.22,\quad P = 0.127 \quad (15)$$

$$\mathbf{25.0\ ^\circ C}: \log D_{Mg} = 0.38 \pm 0.16 \log R^* - 4.34 \pm 0.51,\quad R^2 = 0.77,\quad P = 3.82E-04 \quad (16)$$

$$\mathbf{12.5\ ^\circ C}: \log D_{Mg} = 0.66 \pm 0.18 \log R^* - 5.04 \pm 0.53,\quad R^2 = 0.90,\quad P = 2.58E-05 \quad (17)$$

D_{Mg} values may also depend on [Mg] because the D_{Mg} values of samples 9 (450 mM) and 10 (60 mM) precipitated at 25 °C (marked by arrows in Fig. 4) are much higher when compared to the other samples precipitated at the same temperature but with [Mg] values of only 30 mM.

3.4. Strontium and calcium isotopes

The $\delta^{88/86}Sr$ value of the bulk solution was measured to be 0.173 ± 0.002‰ ($n = 4$) and $\delta^{44/40}Ca = 0.98 \pm 0.09$‰ ($n = 20$), respectively. In order to guarantee comparability of data we are reporting Sr and Ca isotopic fractionation in the Δ-notation: $\Delta^{88/86}Sr_{aragonite\text{-}aq} = \delta^{88/86}Sr_{aragonite} - \delta^{88/86}Sr_{aq}$ and $\Delta^{44/40}Ca_{aragonite\text{-}aq} = \delta^{44/40}Ca_{aragonite} - \delta^{44/40}Ca_{aq}$ (aq = initial solution), respectively. All Δ-values are corrected for the Rayleigh distillation effect (AlKhatib and Eisenhauer, 2017).

Table 4
Initial rate (R), normalized rate to surface area (R^*), saturation index with respect to different carbonates (SI), strontium distribution coefficient (D_{Sr}), magnesium distribution coefficient (D_{Mg}), uncorrected and corrected values for $\Delta^{88/86}Sr$ and $\Delta^{44/40}Ca$.

Sample label	Initial rate (R)/mM/h	1σ Uncertainty/mM/h	Normalized rate (R^*)/μmole/m^2 h	Log R^*	SI. ACC	SI. aragonite	SI. $SrCO_3$	D_{Sr}	Log D_{Sr}	±(2SEM)	$10-^3$ * D_{Mg}	Log D_{Mg}	±(2 SEM)	$\Delta^{88/86}Sr$ (‰) uncorrected	$\Delta^{88/86}Sr$ (‰) corrected	±(2SEM)	$\Delta^{44/40}Ca$ (‰) uncorrected	$\Delta^{44/40}Ca$ (‰) corrected	±(2 SEM)	$[Mg^{2+}]_0$ (mM)	$[Mg^{2+}]_f$ (mM)
1	**2**	**3**	**4**	**5**	**6**	**7**	**8**	**10**	**11**	**12**	**14**	**15**	**16**	**17**	**18**	**19**	**20**	**21**	**22**	**23**	**24**
50C	11.86	0.11	6178	3.79	1.92	1.92	3.00	1.031	0.013	0.003	0.834	−3.079	0.007	−0.110	−0.219	0.010	−1.00	−1.96	0.09	30.16	30.12
50D	7.43	0.15	3488	3.54	2.08	2.09	2.86	1.026	0.011	0.001	0.934	−3.030	0.008	−0.080	−0.194	0.014				30.13	30.09
51E	7.49	0.12	5130	3.71	1.56	1.56	2.64	1.040	0.017	0.006	0.652	−3.185	0.014	−0.127	−0.193	0.012	−1.15	−1.72	0.17	30.19	30.18
51F	5.86	0.00	3745	3.57	1.61	1.62	2.39	1.034	0.015	0.008	0.659	−3.181	0.013	−0.131	−0.210	0.014	−0.67	−1.07	0.17	30.48	30.46
52G	7.21	0.10	5616	3.75	1.65	1.65	2.42	1.033	0.014	0.004	0.673	−3.172	0.013	−0.153	−0.212	0.012	−1.06	−1.45	0.13	30.33	30.32
52H	3.95	0.09	4176	3.62	1.60	1.60	2.68	1.028	0.012	0.005	0.670	−3.174	0.008	−0.167	−0.209	0.013	−1.11	−1.39	0.18	30.39	30.38
24A	2.19	0.09	1398	3.15	1.44	1.45	2.53	1.004	0.002	0.013	0.528	−3.278	0.013	−0.140	−0.208	0.012	−0.60	−0.90	0.10	30.48	30.47
24 B	1.87	0.21	1294	3.11	1.33	1.34	2.13	0.978	−0.01	0.007	0.547	−3.262	0.005	−0.131	−0.187	0.007				30.47	30.46
25D	5.98	0.00	2771	3.44	1.89	1.89	2.67	1.009	0.004	0.004	0.925	−3.034	0.006	−0.096	−0.219	0.015				30.41	30.37
26E	3.52	0.00	1680	3.23	1.68	1.69	2.77	1.011	0.005	0.005	0.518	−3.286	0.006	−0.081	−0.180	0.018				30.26	30.24
26F	2.70	0.03	1500	3.18	1.59	1.59	2.38	0.981	−0.009	0.005	0.764	−3.117	0.004	−0.109	−0.191	0.012				30.17	30.15
27H	4.04	0.28	2227	3.35	1.61	1.61	2.70	1.007	0.003	0.006	0.695	−3.158	0.007	−0.094	−0.172	0.015				30.36	30.34
28A	0.59	0.08	700	2.85	1.07	1.21	2.31	1.099	0.041	0.011	0.562	−3.251	0.009	−0.157	−0.196	0.006				30.19	30.18
28B	0.71	0.04	760	2.88	1.06	1.20	2.00	1.148	0.06	0.011	0.468	−3.329	0.011	−0.138	−0.177	0.008	−1.34	−1.66	0.10	30.17	30.16
29C	2.61	0.14	1613	3.21	1.26	1.40	2.50	1.092	0.038	0.005	0.804	−3.094	0.004	−0.124	−0.214	0.010				30.33	30.31
29D	2.20	0.29	1565	3.19	1.09	1.23	2.02	1.122	0.05	0.003	0.646	−3.190	0.006	−0.132	−0.206	0.019				30.33	30.32
30E	2.22	0.20	1490	3.17	1.02	1.16	2.26	1.114	0.047	0.004	0.750	−3.125	0.005	−0.128	−0.212	0.015	−1.07	−1.64	0.18	30.36	30.34
30F	2.64	0.22	1621	3.21	1.07	1.21	1.99	1.129	0.053	0.005	0.727	−3.138	0.005	−0.127	−0.217	0.009	−0.97	−1.57	0.15	30.02	30.00
31A	6.50	0.44	2845	3.45	1.65	1.79	2.89	1.134	0.055	0.004	0.915	−3.039	0.008	−0.064	−0.229	0.018				30.15	30.10
31B	5.52	0.23	2446	3.39	1.55	1.69	2.49	1.149	0.06	0.004	0.695	−3.158	0.010	−0.063	−0.214	0.021				30.27	30.23
49A	10.52	0.43	6827	3.83	1.38	1.52	2.30	1.107	0.044	0.004	1.131	−2.947	0.006	−0.143	−0.234	0.010	−0.96	−1.51	0.10	30.33	30.30
49B	6.25	0.24	3905	3.59	1.47	1.61	2.38	1.101	0.042	0.006	1.334	−2.875	0.011	−0.137	−0.232	0.012				30.51	30.48
9	5.09	0.39	1837	3.26	1.94	1.34	3.20	1.150	0.061	0.012	1.298	−2.887	0.009	−0.198	−0.208	0.007	−1.49	−1.55	0.20	449.67	449.63
10	2.20	0.11	940	2.97	1.33	1.40	2.66	1.075	0.031	0.008	1.590	−2.798	0.007	−0.167	−0.249	0.009	−1.16	−1.62	0.20	59.97	59.92
11	1.50	0.19	915	2.96	0.93	1.07	2.29	1.067	0.028	0.005	0.688	−3.162	0.008	−0.118	−0.247	0.019				29.94	29.92
32A	0.33	0.05	241	2.38	0.34	0.65	1.76	1.260	0.100	0.011	0.367	−3.436	0.013	−0.129	−0.195	0.011				30.47	30.46
32B	0.72	0.12	832	2.92	0.49	0.79	1.61	1.228	0.089	0.01	0.660	−3.181	0.011	−0.173	−0.216	0.011	−1.24	−1.50	0.19	30.12	30.11
33C	0.58	0.02	710	2.85	0.57	0.88	2.00	1.192	0.076	0.01	0.654	−3.184	0.017	−0.169	−0.204	0.012	−1.41	−1.69	0.15	30.17	30.16
33D	0.53	0.15	601	2.78	0.52	0.82	1.64	1.239	0.093	0.009	0.679	−3.168	0.018	−0.164	−0.208	0.009				30.54	30.53
34E	1.46	0.23	923	2.97	0.72	1.02	2.13	1.202	0.08	0.006	0.896	−3.048	0.009	−0.127	−0.217	0.007				30.53	30.51
34F	2.55	0.01	1419	3.15	0.77	1.08	1.88	1.188	0.075	0.004	0.825	−3.084	0.010	−0.119	−0.240	0.016				30.78	30.75
35A	1.45	0.02	1641	3.22	0.52	0.82	1.95	1.184	0.073	0.012	1.230	−2.910	0.013	−0.169	−0.218	0.006	−1.16	−1.43	0.23	29.77	29.76
35B	1.38	0.06	1104	3.04	0.59	0.89	1.72	1.225	0.088	0.009	0.996	−3.002	0.013	−0.141	−0.218	0.020	−1.10	−1.55	0.17	29.89	29.87
36C	2.25	0.14	1935	3.29	0.71	1.01	2.14	1.176	0.071	0.009	1.567	−2.805	0.008	−0.162	−0.235	0.012	−1.04	−1.42	0.13	30.22	30.19
36D	3.04	0.16	1911	3.28	0.88	1.19	2.01	1.200	0.079	0.002	1.550	−2.810	0.005	−0.129	−0.242	0.011	−0.81	−1.34	0.13	30.31	30.26

Notes: For all reactions the initial rate (mM/h) was calculated according to the initial rate law (see text). R^* = (column 21 Table 1/column 23 Table 1) * column 2. SI of different minerals (columns 5, 7 and 8) are calculated as in the text 3.1. D_{Sr} and D_{Mg} are calculated from Usdowski (1975). **Columns 17** and **20**: these columns show the measured isotope values of Sr and Ca respectively, uncorrected for the reservoir effect. **Columns 18** and **21**: are the corrected values of columns **17** and **20** respectively as described in the text.

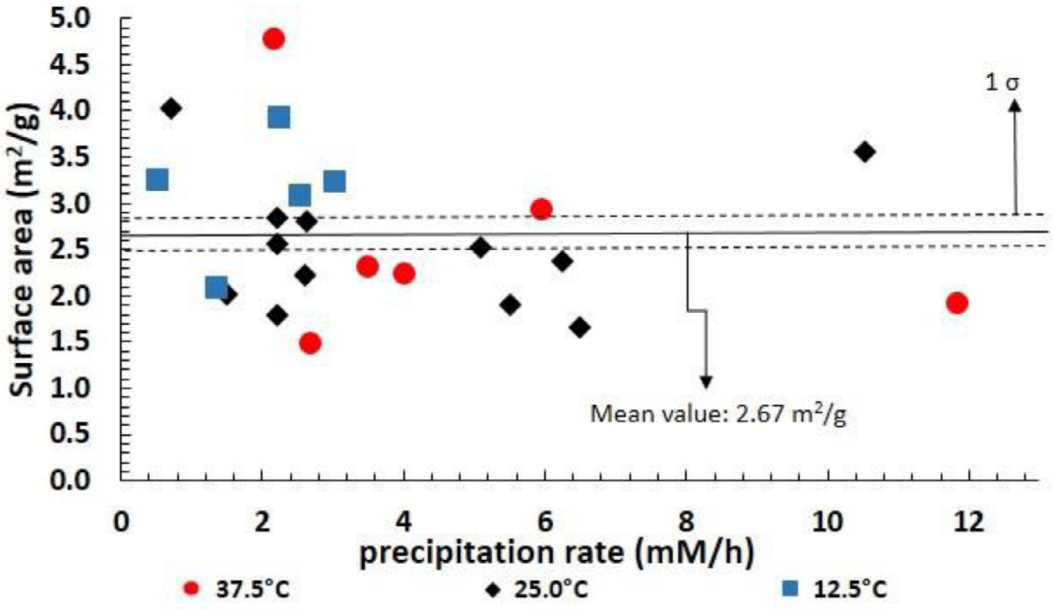

Fig. 2. Specific surface area (S) determined by the BET method (BET = Brunauer-Emmett-Teller gas adsorption method) of some aragonite precipitates versus precipitation rate (R, mM/h) at different temperatures. The value of S is independent of both temperature and precipitation rate and corresponds to 2.7 ± 0.2 m^2/g. Solid line represents the mean value and the dashed lines marks the 1σ-uncertainty of the mean ($n = 23$).

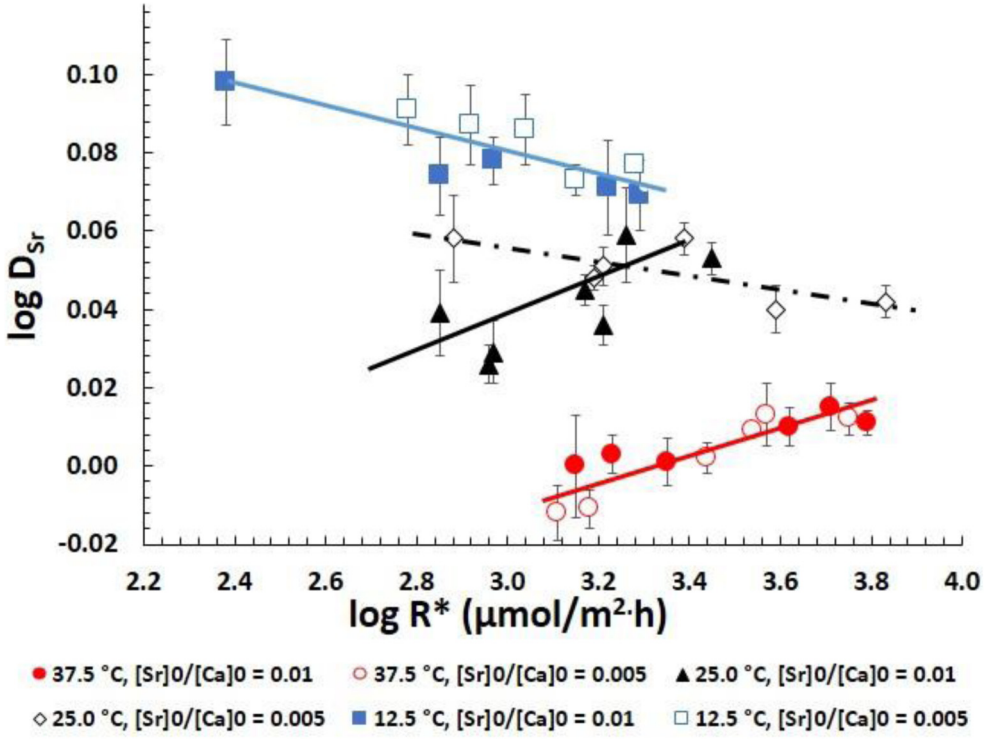

Fig. 3. Log D_{Sr} versus log R^* (µmol/m^2 h) of aragonite precipitated at different temperatures. It can be seen that the relation of log R^* is different for certain temperatures and rates. In particular, this figure shows a separate effect of temperature and precipitation rate.

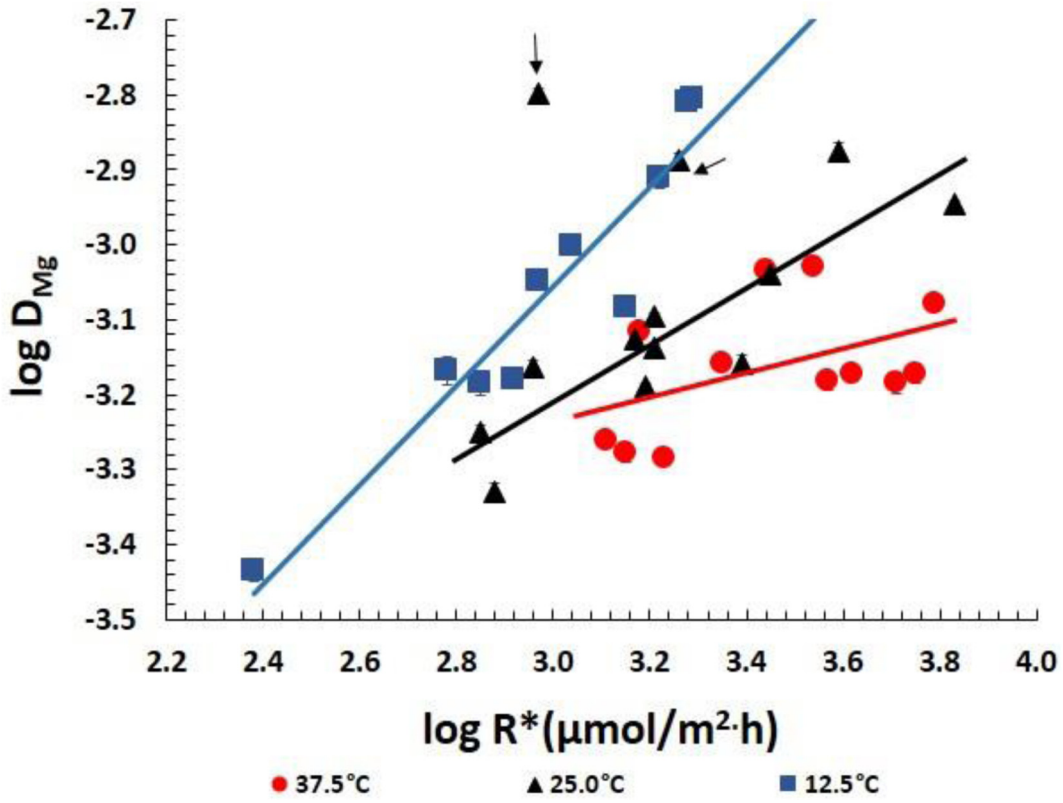

Fig. 4. This figure shows log D_{Mg} at different temperatures versus log R^* (µmol/m^2 h). The log D_{Mg} values increase with increasing R^* and with decreasing temperature, clearly indicating that there is a separate effect of temperature and R^*. Note: black triangles represent reactions 9 and 10 (marked by arrows) at 25.0 °C which have higher Mg^{2+} concentration (430 and 60 mM respectively) and show higher D_{Mg} values.

Uncorrected and corrected values of $\Delta^{88/86}Sr_{aragonite\text{-}aq}$ and $\Delta^{44/40}Ca_{aragonite\text{-}aq}$ are summarized in Table 4.

As it can be seen for the Sr isotopes for all temperatures in Fig. 5 and Table 4 as R^* increases $\Delta^{88/86}Sr_{aragonite\text{-}aq}$-values become more negative. This implies that more light Sr isotopes will become incorporated into aragonite with increasing R^*. In addition there is no effect of the initial ratio $[Sr]/[Ca]_{0,aq}$ on Sr isotopic fractionation. However, at 25 °C two values (samples 10 and 11) show unexpectedly low $\Delta^{88/86}Sr$ without any particular reason. Therefore a lab error cannot be excluded and the Sr isotope values of samples 10 and 11 are arbitrarily neglected for further discussions. All Sr isotope data are again summarized in Fig. 5d emphasizing the role of the temperature. At constant R^* the $\Delta^{88/86}Sr_{aragonite\text{-}aq}$ values decrease at a function of decreasing temperature. At constant temperature $\Delta^{88/86}Sr_{aragonite\text{-}aq}$ values decrease with increasing rate.

From Fig. 6a and b for the Ca isotopes at 12.5 and 25.0 °C as R^* increases $\Delta^{44/40}Ca_{aragonite\text{-}aq}$ tend to become more positive. The slope of the 12.5 °C curve tends to be slightly steeper than the one of the 25 °C curve. In contrast, the Ca isotope fractionation behavior is opposite at 37.5 °C as R^* increases $\Delta^{44/40}Ca_{aragonite\text{-}aq}$ becomes more negative (Fig. 6c). Summarizing the results in Fig. 6d shows no systematic change of $\Delta^{44/40}Ca_{aragonite\text{-}aq}$ values as function of temperature in the range of 12.5–25.0 °C on. However at 37.5 °C the slope of the data is opposite to those at the lower temperatures and tends to be much more sensitive to temperature covering a wider data interval when compared to the low temperature values.

4. DISCUSSION

In the following sections we will discuss the chemical behavior of Sr trace element partitioning and Ca as well as Sr isotope fractionation. In particular the change of sign observed for D_{Sr} and the Ca isotopes is of particular interest.

Note, that the concentrations of NH_3 and NH_4 in our experimental setup are relatively high when compared with the concentrations used in Tang et al. (2008). Latter fact inhibits the calculations of activity coefficients applying geochemical modeling and the PHREEQC software for our study. Consequently, all calculations and model approaches are based on concentrations only.

4.1. Processes driving and inhibiting trace element uptake in aragonite

Concerning calcite the activation energy E_a is found to be ~114 kJ/mol in the absence of Mg^{2+} ions (AlKhatib and Eisenhauer, 2017), while we found in this study that E_a is ~149 kJ/mol for aragonite formation in the presence of Mg^{2+}-ions in solution (Mg/Ca ~ 3). This means that the presence of ~30 mM of Mg^{2+} ions in the reacting solution diminishes calcite formation by increasing E_a to be

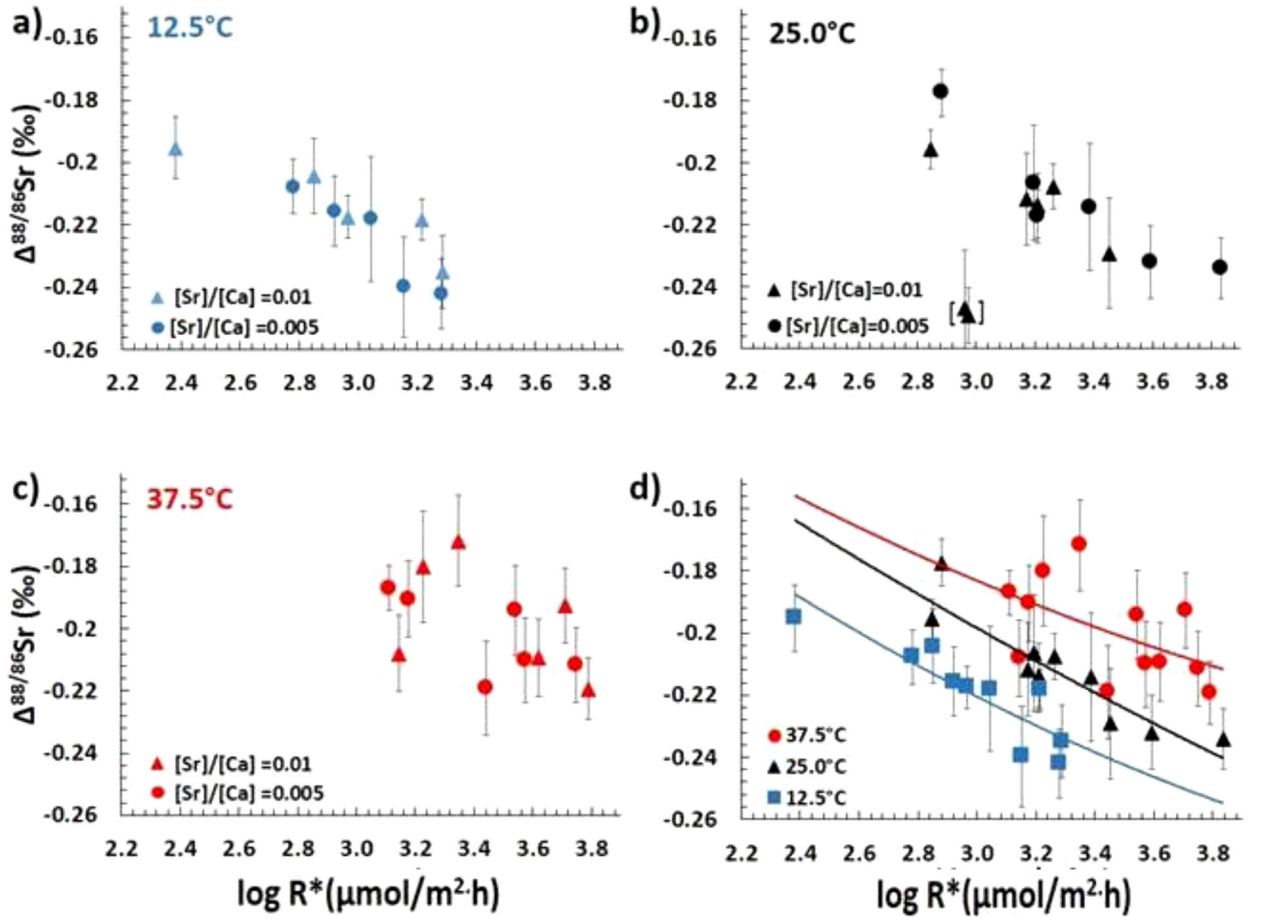

Fig. 5. This diagram shows all $\Delta^{88/86}Sr_{aragonite\text{-}aq}$ values as a function of R^*. For all temperatures, as R^* increases $\Delta^{88/86}Sr$ become more negative. (d) This diagram summarizes the data emphasizing the role of temperature and showing that at constant R^* the initial $\Delta^{88/86}Sr_{aragonite\text{-}aq}$ increases as a function of increasing temperature. Note: results of samples 10 and 11 being part of the 25 °C experiment and marked in brackets are unexpectedly low without any particular reason. Therefore a lab error cannot be excluded and samples 10 and 11 will be neglected for further discussions.

higher than at least ~149 kJ/mol, then favoring aragonite to precipitate rather than calcite.

Beside E_a which is the same for all ions most important for the uptake of ions from solution among others is the individual dehydration energy for a trace metal ion to become released from its corresponding aquacomplex. The dehydration energy (Irving and Williams, 1953; Rodriguez-Cruz et al., 1999) is a function of various parameters and decrease in aquatic solutions from Mg (1921 kJ/mol) via Ca (1577 kJ/mol) to Sr (1443 kJ/mol). Following this approach of the trace elements Sr has the highest probability to be taken up whereas Mg has the least chance to become incorporated into the crystal lattice. In particular, the D_{Sr} values above zero seen in Fig. 3 may reflect the lower dehydration energy of Sr-ions relative to Ca.

A further reason for less Mg present in aragonite when compared to calcite is the number of partners in the crystal lattice. There are six partnering oxygen atoms for calcite but nine for aragonite (Kelleher and Redfern, 2002; Meibom et al., 2004). Simply by volume calcite can accommodate many more Mg atoms and form even high Mg-calcite in contrast to aragonite. Even more because of the low amounts of Mg in aragonite Mg is thought not to become incorporated into the lattice rather is adsorbed only on the surface. As a consequence we consider D_{Mg} more an adsorption rather than a partitioning coefficient.

The presence of larger amounts of Mg^{2+-} ions may have chemical consequences because its tendency to become adsorbed rather than incorporated tends to inhibit calcite nucleation by at least two ways either by increasing the solubility of Mg–calcite (Berner, 1975; Davis et al., 2000) or by increasing the surface energy (γ), since the nucleation barrier energy is proportional to γ^3. It was found that a pristine calcite nuclei shows a γ-energy of 0.21 J/m^2 (Sun et al., 2015), which is lower than the one of aragonite, 0.28 J/m^2 (Sun et al., 2015) confirming that a Mg depleted solution surface energy favors calcite nucleation. However, increasing the [Mg]:[Ca] ratio in the aqueous solution, will linearly increase γ, reaching 0.35 J/m^2 at equilibrium and about 7% $MgCO_3$ concentration of Mg–calcite in modern seawater which than favors the formation of aragonite. Latter effect of increasing γ may have an effect on the uptake of other trace elements e.g. Sr and the isotope fractionation of Sr and Ca, respectively.

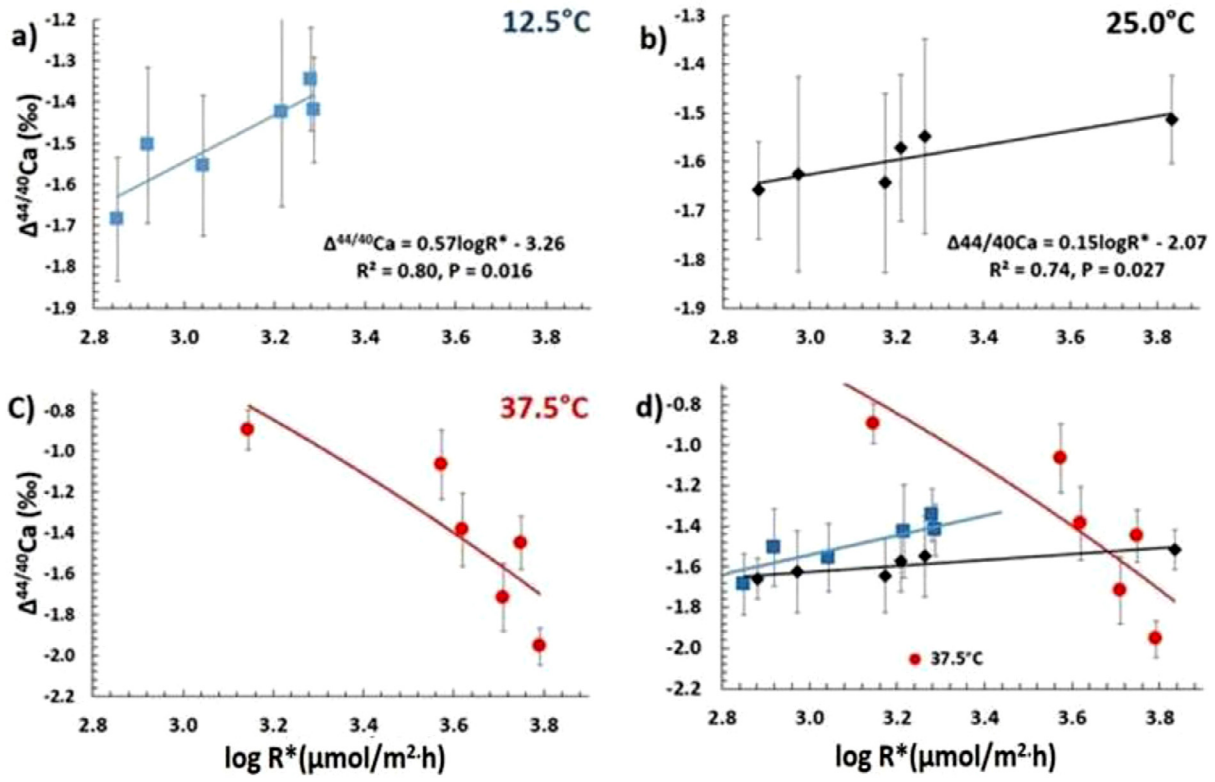

Fig. 6. These figures shows the $\Delta^{44/40}Ca_{aragonite\text{-}aq}$ as function of log R^* at 12.5 (a), 25 °C (b) and 37.5 °C, respectively. For the lower temperatures as rate increase $\Delta^{44/40}Ca_{\ aragonite\text{-}aq}$ become more positive. Note that the slope of the 12.5 °C curve is slightly steeper than the one of the 25 °C curve indicating that the slope of Ca isotope fractionation decreases as a function of temperature. In contrast, at 37.5 °C (c), as R^* increase $\Delta^{44/40}Ca_{\ aragonite\text{-}aq}$ values become more negative in contrast to the values at lower temperatures. Fig 6d emphasizes the strong temperature dependency of the R^* - $\Delta^{44/40}Ca_{aragonite\text{-}aq}$ gradient between 25 and 37.5 °C.

4.2. Ion attachment and detachment from an aragonite crystal surface and the Mg blocking effect

The surface of a crystal consists of flat regions with terraces and raised partial layers called steps (c.f. Chernov, 1961, 1984, 1989). The steps themselves are also incomplete, containing kinks. The kink sites are very important because molecules that attach there make more bonds to neighboring molecules than the ones that attach to the terraces or to flat step edges. Consequently they are more likely to stick. In contrary, when molecules leave the crystal, they can do so more easily by detaching from kinks than from either complete step edges or from embedded sites in the terraces. As a result, the rate at which ions can be added to a crystal, for a given solute concentration, scales with the kink density. This means that the growth rates of crystals can be altered, among other reasons, by either blocking kink sites or by roughening steps (De Yoreo and Vekilov, 2003).

Accumulation of material from a supersaturated solution expressed as a rate (R^*, µmol/m^2 h) occurs because the ion flux attaching to the crystal (R^*_{attach}) surface exceeds the ion flux detaching (R^*_{detach}) from the surface. The probability that an ion will detach from the crystal is solely determined by the strength of its bonds to its neighbors. Since the bond strengths is a function of temperature R^*_{detach} is independent from the concentration in the crystal. In contrast, R^*_{attach} is proportional to the solute supersaturation. Following this approach the solubility product is then the concentration at which R^*_{attach} equals R^*_{detach} and chemical equilibrium is reached (De Yoreo and Vekilov, 2003). However, introduction of distinct elemental impurities, in particular of Mg which is not incorporated rather than adsorbed at the crystal surface at sufficiently high concentrations can alter R^*_{detach}. This is because it sticks at crystal kinks thereby increasing the potential surface energy which increases R^*_{detach} relative to R^*_{attach}. A consequence of this impurity effect knowns as the "Mg blocking effect" it was found that an increase of the Mg concentration in a solution by 20% increases the solubility of calcite from $\log k_{sp} = -8.48$ to $\log k_{sp} = -8.08$ (Davis et al., 2000). Following the mineralogical approach above we infer that the higher aragonite solubility is a function of Mg adsorbed on its surface. Following this approach R^*_{detach} of aragonite is about 40% higher than the one of calcite indicated by the higher solubility of aragonite ($\log k_{sp} = -8.336$) relative to calcite ($\log k_{sp} = -8.480$). As a consequence of higher R^*_{detach} values in aragonite the net R^* value of aragonite is expected to be lower than the net R^* of calcite. These predictions are in general agreement with our observations that at all temperatures $\log R^*$ values for aragonite tend to be 25–30% lower than for calcite ($\log R^*$ mean calcite and aragonite: 3.92 µmole/m^2 h, 3.21 µmole/m^2 h).

Please note that forward (R^*_{attach}) and backward (R^*_{detach}) rates cannot yet individually quantified by any currently

available technique and apparently appear to be untestable. Therefore, the hypothesis put forward here are considered preliminary pending future confirmation by the application of new techniques and methods to separate forward and backward rates of mineral precipitation and dissolution.

4.3. Strontium and calcium incorporation versus magnesium adsorption

Comparing D_{Sr} and D_{Mg} the latter value is about three orders of magnitude lower than the one of Sr (Figs. 3 and 4). Beside the smaller size of the Mg^{2+}-ion (72 pm) relative to the Sr^{2+}-ion (100 pm) presumably this is because of the larger dehydration energy of the Mg^{2+}-aquacomplex (1921 kJ/mol) relative to the Ca^{2+}-aquacomplex (1577 kJ/mol) and the Sr^{2+}-aquacomplex (1443 kJ/mol), respectively. Hence, the probability to overcome E_a and to become incorporated into the crystal is smaller for the Mg^{2+}-ion than for the Ca^{2+}- and Sr^{2+}-ion. Although the dehydration energy of Ca^{2+}-ions is higher than the one of Sr^{2+} the Ca^{2+}-ion is preferentially incorporated because the Ca^{2+}-ion radius fits perfectly well into the $CaCO_3$ lattice in contrast to the Sr^{2+}-ion (Blundy and Wood, 2003). Even more Ca^{2+}-ions are taken up as a function of increasing temperature, supersaturation and the decline of the difference between the kinetic energy of the ions (E_{Kin}) and the dehydration energy (E_a) of the respective aquacomplex. As a consequence D_{Sr} is dropping by about one order of magnitude at constant R^* (Fig. 3). A similar but quantitatively smaller effect can be seen for D_{Mg} as a function temperature from 12.5 to 37.5 °C (Fig. 4).

From Fig. 3 it can be seen that variations of R^* superimpose the decreasing D_{Sr} trend as a function of temperature. For the 12.5 °C data as well at 25 °C (0.005 mmol/mol solution) there is an inverse relationship of the R^*–D_{Sr} values. In contrast at 25 °C (0.01 mmol/mol solution) and the 37.5 °C data there is a positive R^*–D_{Sr} relationship. This change of sign of the gradient is only visible for D_{Sr} but not for D_{Mg}.

The positive trend between R^* and D_{Sr} may be understood to be a consequence of increasing Sr supersaturation (Ω) as a function of increasing R^* generating an enhanced uptake of Sr and potentially a possible enhanced precipitation of $SrCO_3$ within the crystal lattice.

However, this explanation does not hold for the 25 °C (0.005 mmol/mol solution) and the 12.5 °C data where an inverse R^*–D_{Sr} relationship is observed. Following our mineralogical approach concerning the "Mg blocking effect" outlined in Section 4.2 above we may speculate that the increasing D_{Mg} values and absorption of Mg (Fig. 4) on the aragonite crystal surface as a function of R^* lowers the uptake of Sr from the solution thereby lowering R^*_{attach}. This increases the crystal's solubility and R^*_{detach} for Sr becoming larger than R^*_{attach} for Sr (see discussion in Section 4.2). In this case as a function of increasing D_{Mg} the D_{Sr} values are dropping because disproportionally more Sr is leaving the aragonite crystal than can be gained from solution.

The change of sign at 25 °C at a higher Sr/Ca ratio of 0.01 mmol/mol may then reflect a tipping point where increasing Sr supersaturation, increasing temperature and decreasing Mg adsorption out competes the "Mg blocking effect".

4.4. Calcium and strontium isotope fractionation in aragonite

4.4.1. Calcium isotope fractionation

The Ca isotope fractionation in aragonite behaves similar to the one in calcite. As for calcite in our aragonite data there is a positive R^*–$\Delta^{44/40}Ca_{calcite\text{-}aq}$ gradient for the 12.5 and 25 °C data, respectively. However, at 37.5 °C the R^*–$\Delta^{44/40}Ca_{calcite\text{-}aq}$ show an inverse behavior (Fig. 6). Latter observation was already discussed for calcite and will be briefly repeated here. In addition we put forward a second hypothesis (Mg blocking effect) in order to account for the specific chemical settings for aragonite. Our arguments will be among others based on the existences of metal aquocomplexes which we define slightly wider as usually in textbooks as compounds containing metal or also other ions with either water or other dissolved species as ligands.

In order to explain the fractionation behavior of Ca in calcite and aragonite we put forward two hypotheses: the first hypothesis (already put forward in AlKhatib and Eisenhauer (2017)), the temperature dependent Ca^{2+}-NH_3 complexation. In brief we hypothesize that at lower temperatures up to about 25 °C NH_3 complexes with Ca^{2+} to form a Ca^{2+}-NH_3-aquacomplex by a coordinated covalent bonding. The formation constant of this reaction is about 1 (Bjerrum, 1941; Seward, 1954) and the extent of complex formation depends on the concentration of ammonia in the aqueous solution. In order to reach a minimum potential energy in the corresponding oscillation potential between Ca^{2+} and NH_3 and hence to reach a more stable bonding the covalent bonding of the Ca^{2+}-NH_3-aquacomplex prefers the isotopically heavy Ca-isotopes ($\Delta E \approx 1/m$). In this case relatively more light Ca isotopes are statistically available to more easily leave the Ca^{2+}-NH_3 complex to eventually become incorporated into the $CaCO_3$ lattice. Whereas relatively heavier Ca^{2+}-isotopes remain complexed and dissolved in solution. Hence at a certain relatively low temperature and rate the $\Delta^{44/40}Ca_{calcite\text{-}aq}$ value is low because more light Ca isotopes are available for incorporation into the calcite lattice. Increasing DIC concentration and R^*, respectively, will shorten the cross-section and mean free path travel time (Rohlf, 1994) between ions allowing relatively more heavy Ca isotopes to overcome the binding energy of the Ca^{2+}-NH_3-aquacomplex and to become eventually incorporated into the calcite lattice. In this case statistically with increasing rate relative more isotopically heavy Ca^{2+}-ions become available for the incorporation into the crystals lattice. Hence, $\Delta^{44/40}Ca_{aragonite\text{-}aq}$ correlates positively to R^*. Further temperature increase to 37.5 °C the Ca^{2+}-NH_3-aquacomplex will be completely replaced by a Ca^{2+}-H_2O-aquacomplex substituting the NH_3 molecules completely by H_2O molecules. However, the water molecules are not covalently bond rather form a weak van-der-Waals bonding with the Ca^{2+}-ions. Latter electrostatic bonding cannot be related to an equilibrium type like isotope fractionation process where the heavy isotope is preferred in order to reach a minimum potential energy to form a covalent

bonding. In the absence of a covalent bonding only kinetic isotope fractionation can be observed preferring the light isotopes. Hence, as R^* increases more lighter Ca isotopes will be included in aragonite and the $\Delta^{44/40}$Ca values become more negative.

The second hypothesis in order to explain the discrepant behavior of Ca isotope fractionation at 12.5 and 25 °C compared to 37.5 °C depends on the "Mg blocking effect" as described above in Section 4.2. We infer that at lower temperatures at 12.5 and 25 °C when relatively higher amounts

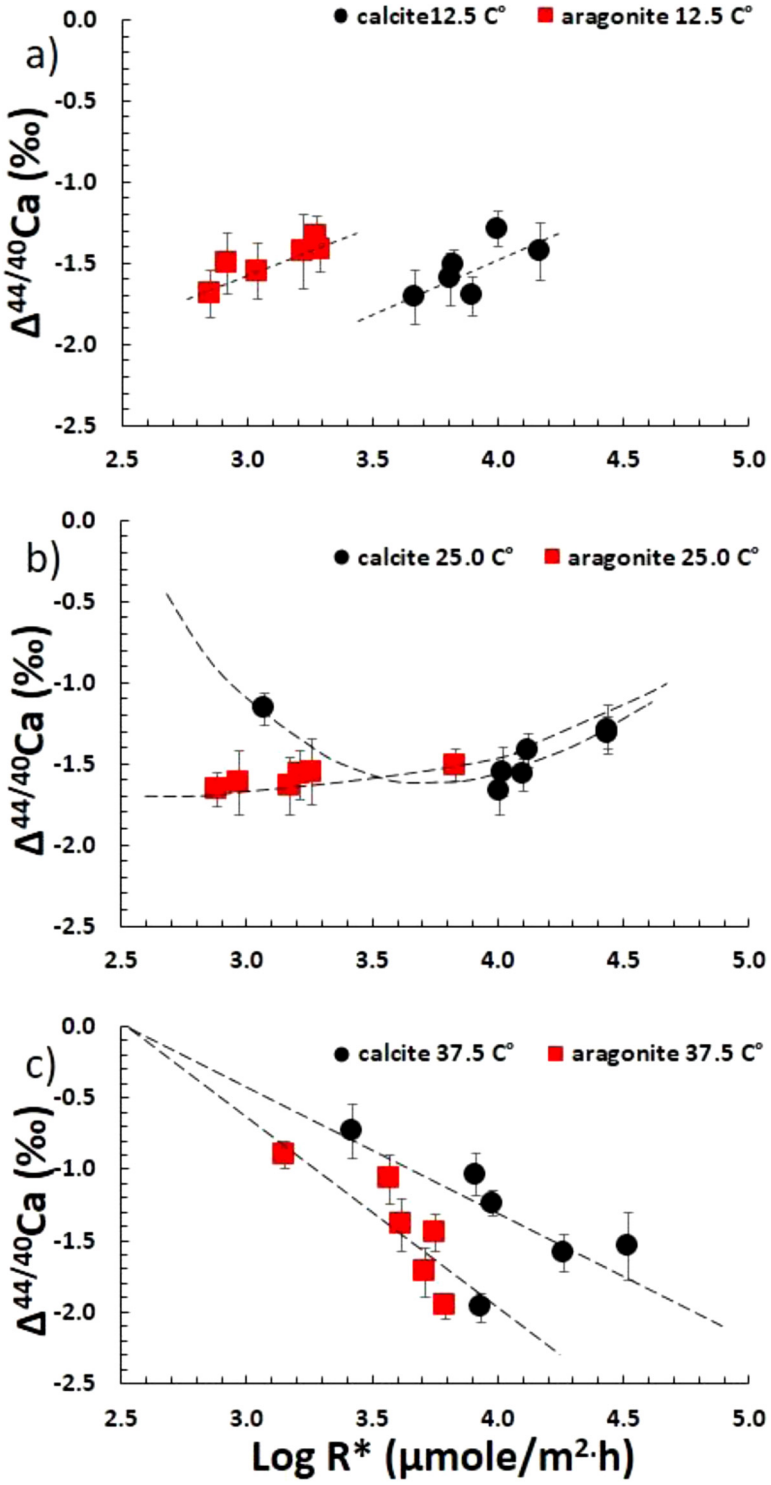

Fig. 7. In (a and b) it can be seen that calcite and aragonite values show indistinguishable $\Delta^{44/40}$Ca values for different R^* being lower for aragonite but higher for calcite. Both calcite and aragonite Ca fractionation behavior change simultaneously at 37.5 °C (Fig. 7c).

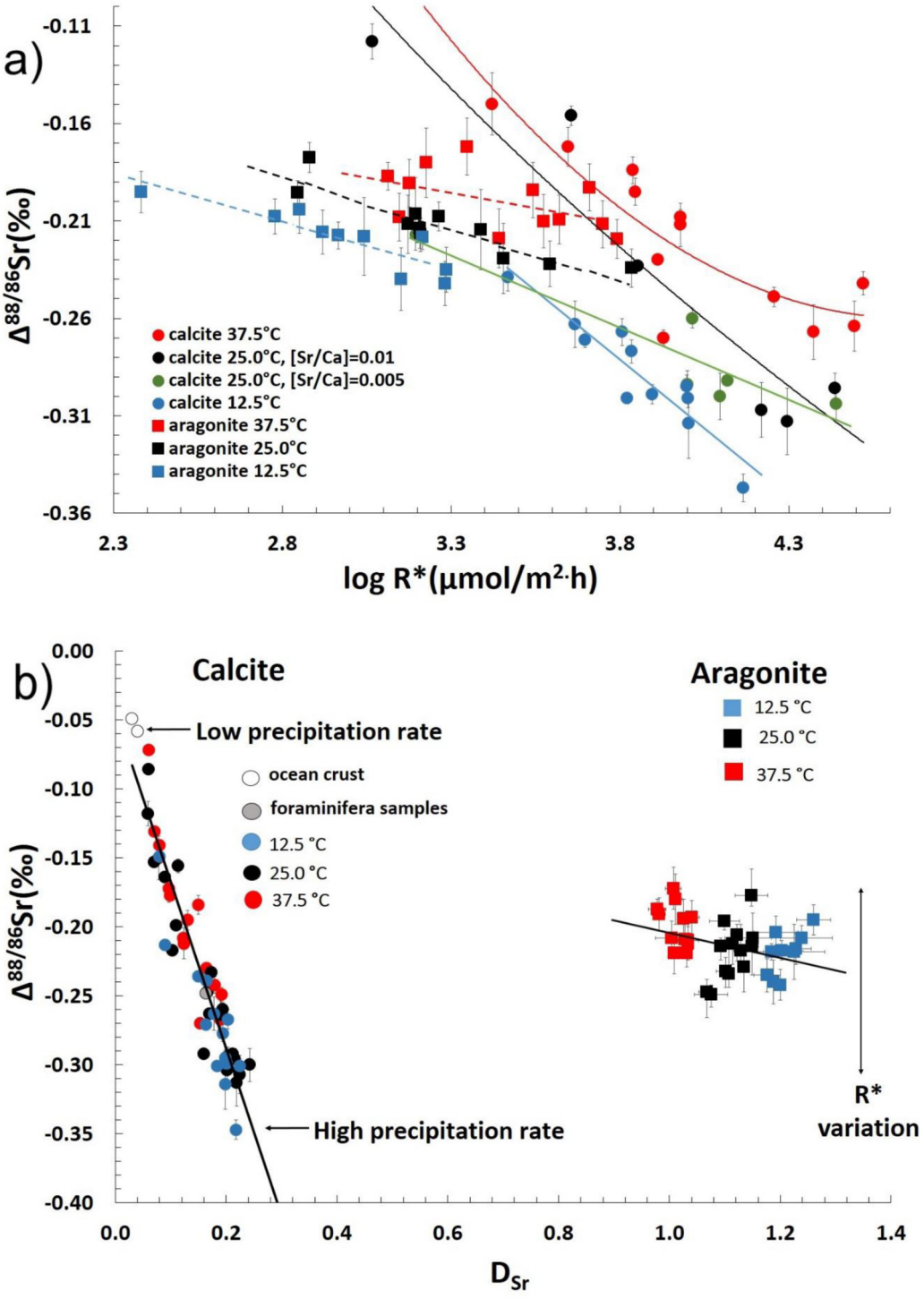

Fig. 8. Comparison between aragonite and calcite. Solid curves represent calcite, while dashed curves represent aragonite. The values shown in this plot combine the data from this study and our earlier study on calcite (AlKhatib and Eisenhauer, 2017). (a) This diagram shows that all $\Delta^{88/86}Sr$ values (for both calcite and aragonite) become more negative as a function of increasing R^*. However the rate effect is larger in calcite as seen from the steepness of the corresponding curves. (b) The linear correlations of $\Delta^{88/86}Sr$ and D_{Sr} for calcite it is dependent only on R^* and is independent of temperature. For aragonite $\Delta^{88/86}Sr$ values are much less sensitive to R^* than to temperature. In contrast to calcite the D_{Sr} - $\Delta^{88/86}Sr$ values correlation depend on temperature.

of Mg (Fig. 4) are blocking kinks and terraces at the surface of the aragonite crystal R^*_{detach} favors the release of isotopically light Ca isotopes to a much larger extent when compared to R^*_{attach}. With increasing temperature and decreasing D_{Mg} and at a tipping point around 25 °C disproportionally more isotopically light Ca isotopes are associ-

ated with R^*_{attach} when compared to R^*_{detach}. Then a temperature around 25 °C marks a tipping point where R^*_{attach} is associated with more lighter Ca isotopes than R^*_{detach}.

Both processes "Ca^{2+}-NH_3 complexation" and the "Mg^{2+} blocking effect" as described above may be favored in our experimental setup. The effect of Ca^{2+}-NH_3 complexation on $\Delta^{44/40}$Ca as a function of R^* is similar in aragonite and calcite (AlKhatib and Eisenhauer, 2017) whereas the "Mg blocking effect" is only interfering with the aragonite precipitation because Mg was completely absent in our calcite experiment. The relative contribution of the two effects "Ca^{2+}-NH_3 complexation" and the "Mg blocking effect" can be further tested when aragonite is precipitated in the absence of NH_3. Then in the case of aragonite any change of sign in the $\Delta^{44/40}$Ca-precipitation rate can be attributed to the "Mg blocking effect" and vice versa.

4.4.2. Strontium isotope fractionation

Similar to the observation in calcite we see a kinetic type of Sr isotope fractionation for all temperatures where isotope fractionation increases and more lighter Sr isotope are taken up as a function of R^*. Obviously NH_3 complexation doesn't have any influence on the Sr isotope fractionation. Probably because of its lower ionic potential based on the larger ionic radius ($Sr^{2+} \sim 132$ pm; $Ca^{2+} \sim 114$ pm) solvation of Sr with water molecules forming a Sr^{2+}-H_2O-aquacomplex is more dominant than covalent binding and forming of a Sr^{2+}-NH_3-aquacomplex during solvation. This is supported by earlier observations that Sr is not complexing with most ligands due to its lower ionization potential when compared to Ca (Irving and Williams, 1953). In this case Sr isotope fractionation favors only kinetic fractionation as it is observed for Ca at 37.5 °C.

5. COMPARISON OF ELEMENT PARTITIONING AND ISOTOPE FRACTIONATION IN ARAGONITE AND CALCITE

5.1. Comparison of calcium isotope fractionation in calcite and aragonite

Simply looking at the Ca isotope fractionation the absolute amount of isotope fractionation is indistinguishable for calcite and aragonite, respectively. From Fig. 7 it can be seen that different complexation either Ca-NH_3 (12.5 and 25 °C) or a usual Ca^{2+}-aquacomplex (at 37.5 °C) complexation did not cause relative variations of Ca isotope fractionation between polymorphs. The only visible difference comes from the different precipitation rates R^* higher for calcite and lower for aragonite due to the "Mg blocking effect" (see discussion in Section 4.3).

There are hardly $\Delta^{44/40}$Ca values above -1.2‰ for the 12.5 and 25 °C data for both calcite and aragonite. Whereas the 37.5 °C data show values above −1.2‰ up to about −0.6‰. Beside the change in the direction of the Ca isotope fractionation (see discussion in Section 4.4.1 above!) the stronger covalent Ca^{2+}-NH_3-complexation is corresponding to more positive $\Delta^{44/40}$Ca values because only light (e.g. ^{40}Ca) ions can disproportionally be desolvated from Ca^{2+}-NH_3-complexation. In this regard a value of −1.2‰ may correspond to a certain threshold value for the dissociation indicating that the dissociation energy for the Ca^{2+}-NH_3-complexation tend to be significantly higher than the one of the Ca^{2+}-aquacomplex.

A major implication of this observation in calcite and its related hypothesis is that the direction of the Ca isotope fractionation as well as the amount of fractionation is independent of the mineralogy rather depends on the type of chemical bonding and complexation in solution.

5.2. Comparison of strontium isotope fractionation in calcite and aragonite

Strontium element partitioning (D_{Sr}) and isotope fractionation in calcite and aragonite differs considerably in their respective R^*–D_{Sr} and R^*–$\Delta^{88/86}Sr_{calcite\text{-}aq}$ gradients, respectively. In particular the R^*–$\Delta^{88/86}Sr_{calcite\text{-}aq}$ gradients are much steeper for calcite than for aragonite (Fig. 8a). The shallow R^*–$\Delta^{88/86}$Sr aragonite gradients as well as the temperature dependency of D_{Sr} is assumed to be associated with the "Mg blocking effect" related to the presence of Mg in solution and adsorption on the aragonite surface, respectively (see discussion in Section 4.3).

The D_{Sr}–R^* relationship is much more complex in aragonite then in calcite changing sign as a function of temperature above ≥25 °C as a function of both temperature and initial Sr/Ca ratios (Fig. 3). Probably this also reflects the "Mg blocking effect", increasing crystals solubility and the enhanced release of crystal lattice bound isotopically light Sr. The "Mg blocking effect" diminishes as a function of rising temperatures, less Mg adsorbed on the aragonite crystal surface and the incorporation of relatively more Ca from the fluid.

The presence of Mg increases aragonite solubility by depressing the uptake of ions from the solution, R^*_{detach} and favors the release of isotopically lighter Sr isotopes from the solid. Latter flux is counter balanced by R^*_{attach} the flux of isotopically lighter Sr isotopes from the solution to the solid. As a consequence of the higher aragonite solubility and the counter balancing effects of R^*_{attach} and R^*_{detach} the interval of Sr isotope fractionation ($\Delta^{88/86}Sr_{calcite\text{-}aq}$: ∼−0.16 to −0.25) for aragonite is smaller than for calcite ($\Delta^{88/86}Sr_{calcite\text{-}aq}$: −0.11 to −0.36) as well as for the R^* values which are significantly lower for aragonite (<3.6 μmole/m^2 h) than for calcite (>3.6 μmole/m^2 h).

The similarities and differences in Sr partitioning and isotope fractionation is one more time emphasized in Fig. 8b. The larger spread of $\Delta^{88/86}Sr_{calcite\text{-}aq}$ values are associated with lower D_{Sr} values for calcite and the considerable lower spread of the $\Delta^{88/86}Sr_{calcite\text{-}aq}$ values are associated with higher D_{Sr} values for aragonite. The D_{Sr} and $\Delta^{88/86}Sr_{calcite\text{-}aq}$ values for calcite are strongly correlated because Sr uptake and Sr isotope fractionation depend only on R^*. Therefore low precipitation rates are associated with low D_{Sr} values and smaller amounts (more positive values) of Sr isotope fractionation. Whereas higher precipitation rates are related to larger D_{Sr} values and more negative $\Delta^{88/86}Sr_{calcite\text{-}aq}$ values. This relationship between R^*, D_{Sr} and $\Delta^{88/86}Sr_{calcite\text{-}aq}$ in calcite is independent of temperature.

In contrast to calcite the spread of the $\Delta^{88/86}Sr_{aragonite\text{-}aq}$ values are much smaller when compared to the calcite data. Both observations can be attributed to the "Mg blocking effect" which controls the solubility for aragonite associated with an increasing loss of Sr as function of temperature. The smaller spread in the $\Delta^{88/86}Sr_{aragonite\text{-}aq}$ values reflect the counterbalancing effect of R^*_{attach} and R^*_{detach} as discussed above in Section 4.3. In contrast to calcite in aragonite there is a general inverse R^*–$\Delta^{88/86}Sr_{calcite\text{-}aq}$ relationship but an ambivalent relationship to D_{Sr}, positive for 25 (0.1 mmol/solution) and 37.5 °C but inverse for the 12.5 and 25 °C (0.05 mmol/mol solution). The contrasting behavior of Sr at 25 °C presumably reflect a tipping point value related to the counter balancing effect of R^*_{attach} and R^*_{detach} as a function temperature.

6. SUMMARY AND CONCLUSIONS

- The $\Delta^{44/40}Ca_{aragonite\text{-}aq}$ fractionation as function of R^* follows the same temperature controlled pattern in both aragonite and calcite. The $\Delta^{44/40}Ca_{aragonite\text{-}aq}$ values in calcite and in aragonite reflect the type and strength of solvation of the Ca^{2+}-ions to their respective ligands either NH_3 or H_2O.
- Neither D_{Sr} nor $\Delta^{88/86}Sr_{calcite\text{-}aq}$ and $\Delta^{88/86}Sr_{aragonite\text{-}aq}$ depend on the type of bonding in the solution. Probably Sr is always forming a Sr^{2+}-H_2O-aquacomplex in solution unlike the observation from Ca.
- The rate law (order of reaction) for the precipitation of $CaCO_3$ is the same for both calcite and aragonite when precipitation is occurring under the same chemical conditions and experimental setup.
- The D_{Sr}–R^* relationship is much more complex in aragonite changing sign above $\geq$25 °C as a function of both temperature and initial Sr/Ca ratios. Probably this reflects the "Mg blocking effect", increasing crystals solubility and the enhanced release of crystal lattice bound isotopically light Sr. The "Mg blocking effect" diminishes as a function of rising temperatures, less Mg adsorbed on the aragonite crystal surface and the incorporation of relatively more Ca from the fluid.
- Similar the D_{Sr}–$\Delta^{88/86}Sr$ gradients changing signs as a function of the contrary effects of the "Mg blocking effect" and temperature. The interval of $\Delta^{88/86}Sr$ values is smaller in aragonite than in calcite because again due to the "Mg blocking effect" and the increased solubility of the aragonite crystal.

ACKNOWLEDGEMENT

This study is part of the joint German-Palestinian-Israeli project (TRION) coordinated by AE in the frame of the "*Trilateral Programm der Deutschen Forschungsgemeinschaft*, DFG (Ei272/30/31-2)" to make a small contribution to the peace process in the Middle East by supporting scientific interaction and communication in a politically difficult environment. Mrs. Ana Kolevica is acknowledged for laboratory help and support in the design of the experiments. For fruitful discussions, Florian Böhm, Volker Liebetrau and Jan Fietzke are acknowledged. Prof. Dr. Mutaz AlQutob from the AlQuds University in AbuDis, Palestinian Authority, Prof. Boaz Lazar and Moti Stein from the Hebrew university of Jerusalem are acknowledged for their general support of the work of MA. We greatly acknowledge the comments and suggestions of three reviewers who considerably helped to improve the manuscript.

APPENDIX A

A.1. Documentation of the prepicitation of aragonite

In Fig. A1 two typical arbitrarily selected XRD spectra are presented as an example that aragonite was precipitated with our experimental setup rather than high Mg-calcite. The first spectra is a typical calcite spectra with a dominant peak at 29.4° 2Θ. The second diagram below shows a typical arbitrarily selected XRD spectra of one of our aragonite samples. Here the aragonite can be recognized from the two dominant peaks at 26.2° 2Θ und 27.2° 2Θ. In addition there are prominent peaks at 33.0° 2Θ and at 45.8° 2Θ. Traces of $SrCO_3$ should be visible at 25.2° 2Θ and at 25.9° 2Θ.

A.2. Calculation of the precipitation rate "R and the rate of reaction "k from the initial rate method

In order to calculate the rate R for all sample reactions we plotted $[Ca^{2+}]$ for all samples as a function of time. For example see randomly selected sample 34F where the change in $[Ca^{2+}]$ as function of time fits the polynomial function ($[Ca^{2+}]$ (mM) = 0.43 (mM/h^2) · t^2 − 3.52 (mM/h) · t + 10.51; Fig. A1). The derivative of this function corresponds to the instantaneous rate R ($[Ca^{2+}]$ (mM/h) = 0.86 (mM/h) · t − 3.52 (mM/h); Fig. A1a). However, for practical reasons the first six points can also be approximated by a linear function ([Ca] = −2.55 (mM/h) · t + 10.26 (Fig. A2a) from which directly the rate R ($R = d[Ca^{2+}]/dt$) can be seen to be 2.55 mM/h. Latter value is constant and a good approximation for the average rate of precipitation because more than 90% of the whole precipitation process corresponds to the linear part of this process.

A.3. The rate law and the order of precipitation for aragonite

In order to calculate the order of reaction (A1) "x" for [Ca] the log of instantaneous rate of precipitation can be plotted as a function of log $[Ca^{2+}]$.

$$R = K[Ca^{2+}]^x \cdot [DIC^-]^y \quad (A1)$$

For simplicity we assume that $DIC \approx [HCO_3^-]$ because for most sample reactions the majority of DIC are bicarbonate ions (see Table 1 column 10). Furthermore, during the course of the experiment the [TA] did not change markedly. In this case we can write:

$$R = K^*[Ca]^x; K^* = K[HCO_3^-]^y \quad (A2)$$

The initial concentration of $[Ca^{2+}]^x$ is initially set constant at about 10 mM but changes as a function of the amount

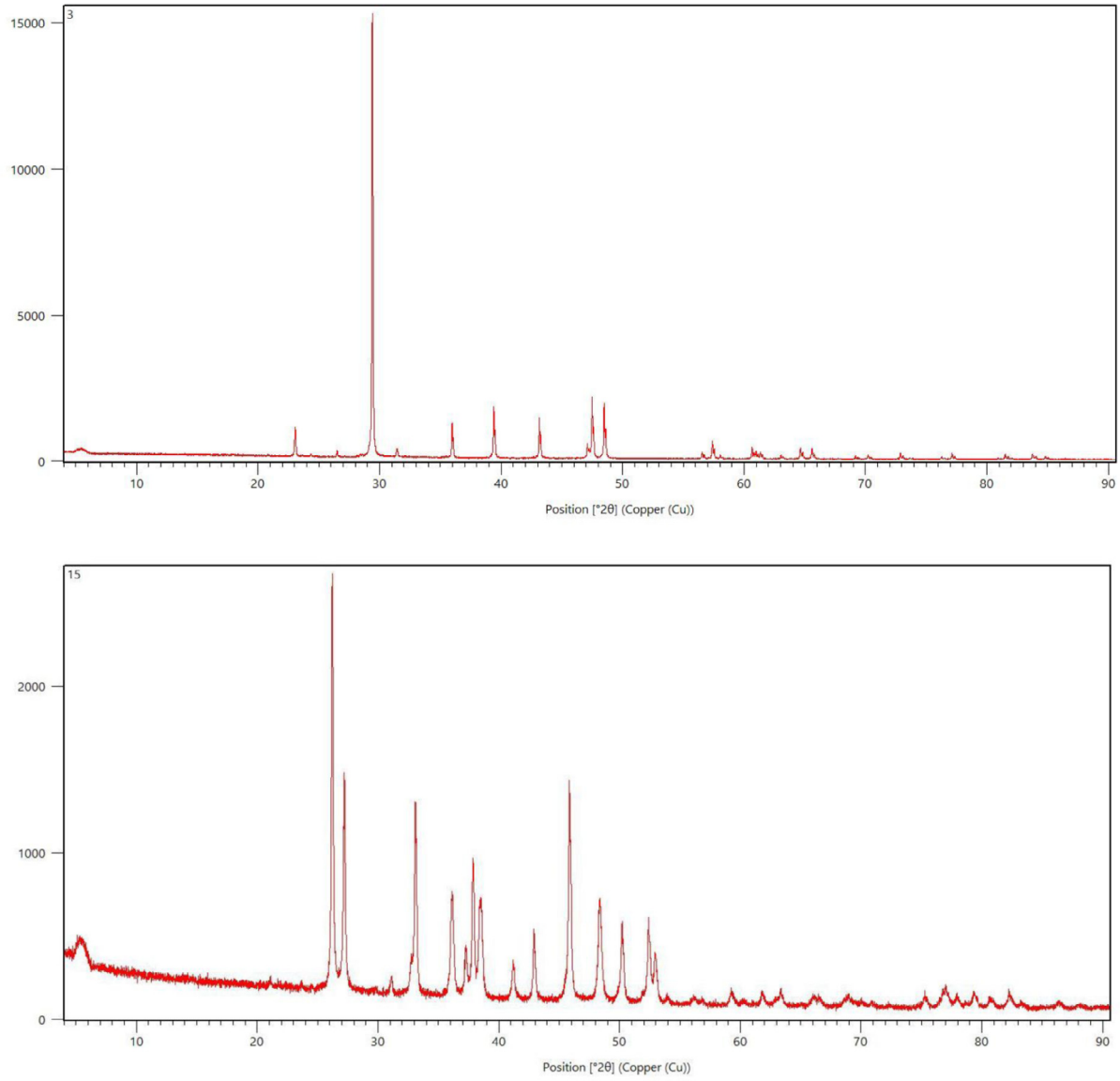

Fig. A1. In figure A1 two typical XRD spectra are presented as an example for a typical calcite spectra (AlKhatib and Eisenhauer, 2017) with a dominant peak at 29.4° 2Θ. The second diagram shows a typical XRD spectra of one of our aragonite samples. Here the aragonite can be recognized from the two dominant peaks at 26.2° 2Θ und 27.2° 2Θ. In addition there are prominent peaks at 33.0° 2Θ and at 45.8° 2Θ. Traces of strontianite should be visible at 25.2° 2Θ and at 25.9° 2Θ.

precipitated from the solution. Following this approach Eq. (A1) can be written as:

$$\log\ R = \log\ K^{*} + x\log[Ca^{2+}] \tag{A3}$$

In this equation the term ($K^{*} = K\ [HCO_3^{-}]^{y}$) is considered to be constant and corresponds to a value of −0.45 mM for experiment 34F (see Fig. A3). The order of reaction "x" concerning calcium then corresponds to the slope of this relationship and can be calculated to be close to one (see Fig. A3). Repeating this calculation for all other precipitation experiments showed that values for "x" vary between 0.65 and 1.3. All together correspond to an average order of reaction "x" with respect to [Ca] to be about 1.0 ± 0.2 (see Fig. A3).

Following the same approach the order of reaction "y" with respect to the DIC (here $[DIC] \approx [HCO_3^{-}]$) can be calculated from the three temperature experiments keeping [Ca] constant because the initial [Ca] was set to 10 mM for all experiments:

$$R = K^{*}[HCO_3^{-}]^{y};\quad K^{*} = K[Ca^{2+}]^{x} \tag{A4}$$

by plotting "R" as a function of the initial $[DIC] \approx [HCO_3^{-}]$ concentrations for all temperatures the order of reaction

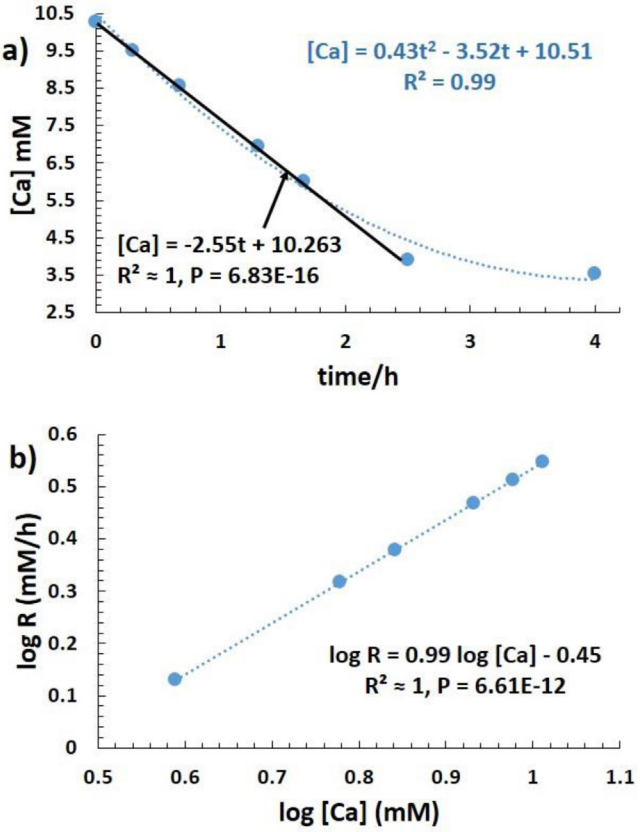

Fig. A2. In (a) the decrease of the [Ca] concentration in the solution due to $CaCO_3$ precipitation is shown as a function of time. The decline can be approximated by a quadratic polynomial (blue) and a linear function (black). The derivative of the quadratic polynomial function represents the instantaneous rate of reaction. Whereas the derivate of the linear function equals the precipitation rate R and can be taken as an average value for the precipitation rate of the whole reaction. In (b) the instantaneous rate of reaction (log R) is plotted as a function of log [Ca]. Latter relationship can be applied to calculate the rate constant "x" corresponding to the aragonite precipitation.

for the precipitation reaction with respect of the carbonates can be calculated:

$$\log\ R = \log\ K^* + y\log[HCO_3^-] \quad (A5)$$

Results for the three temperatures show that the order of reaction decreases from about 3 at 12.5 °C, via 2 for 25 °C to 1 at 37.5 °C.

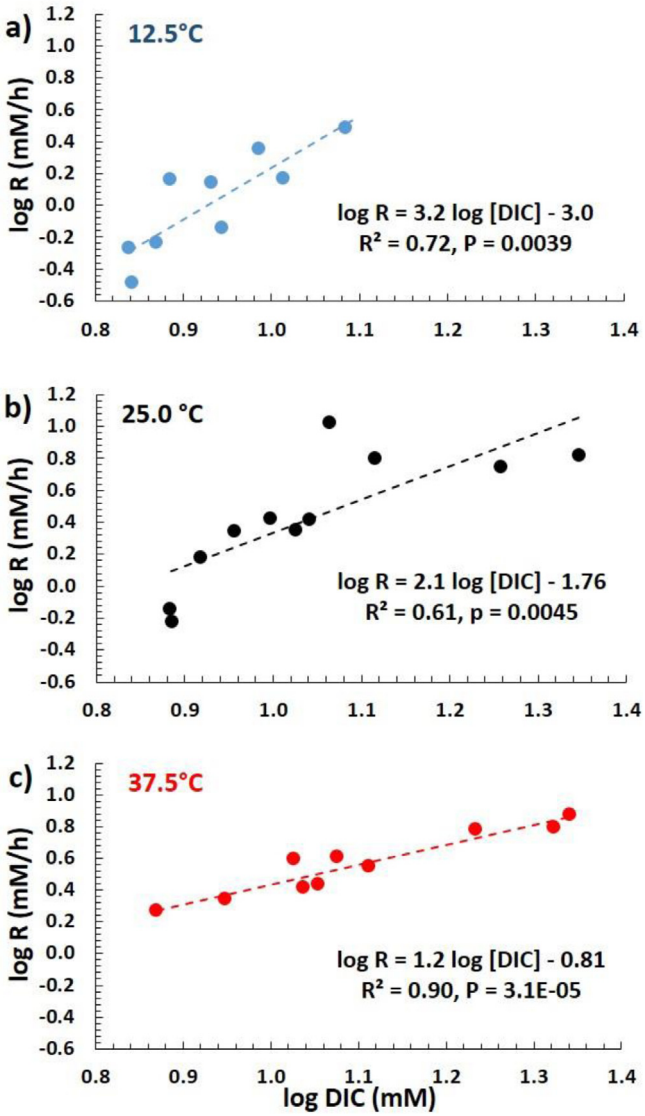

Fig. A3. In this figure $\Delta^{44/40}$Ca is plotted as a function of [DIC] for the three temperatures. The derivative of the linear function then corresponds to the order of reaction "*y*" with respect to [DIC]. Unlike for [Ca] it can be seen that that the order of reaction is temperature dependent decreasing from about one via two to three as temperature increase from 12.5, 25 and 37.5 °C.

REFERENCES

Alkhatib M. and Eisenhauer A. (2017) Calcium and strontium isotope fractionation in aqueous solutions as a function of temperature and reaction rate. Geochem. Cosmochem. Acta.

Beck J. W., Edwards R. L., Ito E., Taylor F., W. Recy J., Rougerie F., Joannot P. and Hening C. (1992) Sea-surface temperature from coral skeletal strontium calcium ratios. Science 257(5070), 644–647.

Berner R. A. (1975) The role of magnesium in the crystal growth of calcite and aragonite from seawater. *Geochim. Cosmochim. Acta* **39**, 489–504.

Bjerrum J. (1941) *Metal Ammine Formation in Aqueous Solutions*. P. Haase and Son, Copenhagen, p. 147.

Blundy J. and Wood B. (2003) Partitioning of trace elements between crystals and melts. *Earth Planet. Sci. Lett.* **6607**, 1–15.

Böhm F., Gussone N., Eisenhauer A., Dullo W. C., Reynaud S. and Paytan A. (2006) Calcium isotope fractionation in modern scleractinian corals. *Geochem. Cosmochem. Acta* **70**, 4452–4462. http://dx.doi.org/10.1016/j.gca.2006.06.1546.

Böhm F., Eisenhauer A., Tang J. W., Dietzel M., Krabbenhöft A., Kisakürek B. and Horn C. (2012) Strontium isotope fractionation of planktic foraminifera and inorganic calcite. *Geochim. Cosmochim. Acta* **93**, 300–314.

Burton E. A. and Walter L. M. (1987) Relative precipitation rates of aragonite and Mg calcite from seawater: temperature or carbonate ion control? *Geology* **15**, 111–114.

Busenberg E., Plummer L. N. and Paker V. B. (1984) The solubility of strontianite ($SrCO_3$) in CO_2-H_2O solutions between 2 and 91 °C the association constants of $SrHCO_3^+$(aq) and $SrCO_3^0$(aq) between 5 and 80 °C and an evaluation of the thermodynamic properties of Sr^{2+} (aq) and $SrCO_3$ (cr) at 25 °C and 1 atm total pressure. *Geochim. Cosmochim. Acta* **48**, 2021–2035.

Chernov A. A. (1961) The spiral growth of crystals. *Sov. Phys. Uspekhi* **4**, 116–148.

Chernov A. A. (1984) *Modern Crystallography III: Crystal Growth*. Springer, Berlin.

Chernov A. A. (1989) Formation of crystals in solutions. *Contemp. Phys.* **30**, 251–276.

Clarkson J. R., Price T. J. and Adams C. J. (1992) Role of metastable phases in the spontaneous precipitation of calcium carbonate. *J. Chem. Soc. Faraday Trans.* **88**(2), 243–249.

Davis K. J., Dove P. M. and De Yoreo J. J. (2000) Resolving the controversial role of Mg^{2+} in calcite biomineral formation. *Science* **290**, 1134–1137.

De Kanel J. and Morse J. W. (1979) A simple technique for surface area determination. *J. Phys. E: Sci. Instrum.* **12**, 272–273.

De Villiers S., Shen G. T. and Nelson B. K. (1994) The Sr/Ca temperature relationship in coralline aragonite—influence of variability in (Sr/Ca) seawater and skeletal growth-parameters. *Geochim. Cosmochim. Acta* **58**(1), 197–208.

De Yoreo J. J. and Vekilov P. G. (2003) Principles of crystal nucleation and growth. *Rev. Mineral. Geochem.*, 57–93.

Dietzel M., Gussone N. and Eisenhauer A. (2004) Precipitation of aragonite by membrane diffusion of gaseous CO_2 and the coprecipitation of Sr^{2+} and Ba^{2+} (10 to 50 °C). *Chem. Geol.* **203**, 139–151.

Eisenhauer A., Kisakürek B. and Böhm F. (2009) Marine calcification: an alkaline earth metal isotope perspective. *Elements* **5**(6), 365–368.

Enmar R., Stein M., Bar-Matthews M., Sass E., Katz A. and Lazar B. (2000) Diagenesis in live corals from the Gulf of Aqaba. I. The effect on paleo-oceanography tracers. *Geochim. Cosmochim. Acta* **64**(18), 3123–3132.

Fantle M. S. and Higgins J. (2014) The effects of diagenesis and dolomitization on Ca and Mg isotopes in marine platform carbonates: implications for the geochemical cycles of Ca and Mg. *Geochim. Cosmochim. Acta* **142**, 458–481.

Fruchter N., Eisenhauer A., Dietzel M., Fietzke J., Böhm F., Montagna P., Stein M., Lazar B., Rodolfo-Metalpa R. and Erez J. (2016) $^{88}Sr/^{86}Sr$ fractionation in inorganic aragonite and in corals. *Geochem. Cosmochem. Acta* **178**, 268–280.

Gabitov R. I., Gaetani G. A., Watson E. B., Cohen A. L. and Ehrlich H. L. (2008) Experimental determination of growth rate effect on U^{6+} and Mg^{2+} partitioning between aragonite and fluid at elevated U^{6+} concentration. *Geochim. Cosmochim. Acta* **72**, 4058–4068.

Gabitov R. I. (2013) Growth-rate induced disequilibrium of oxygen isotopes in aragonite: an in situ study. *Chem. Geol.* **351**, 268–275.

Gaetani G. A. and Cohen A. L. (2006) Element partitioning during precipitation of aragonite from seawater: a framework for understanding paleoproxies. *Geochim. Cosmochim. Acta* **70**, 4617–4634.

Greegor R. B., Pingitore, Jr, N. E. and Lytle F. W. (1997) Strontianite in coral skeletal aragonite. *Science* **275**, 1452–1454.

Gussone N., Eisenhauer A., Heuser A., Dietzel M., Bock B., Böhm F., Spero H. J., Lea D. W., Bijma J. and Nägler T. F. (2003) Model for kinetic effects on calcium isotope fractionation ($\delta^{44}Ca$) in inorganic aragonite and cultured planktonic foraminifera. *Geochim. Cosmochim. Acta* **67**, 1375–1382.

Gutjahr A., Dabringhaus H. and Lacmann R. (1996) Studies of the growth and dissolution kinetics of $CaCO_3$ polymorphs calcite and aragonite I. Growth and dissolution rates in water. *J. Cryst. Growth* **158**, 296–309.

Hathorne Ed. C., Gagnon A. and Felis T., et al. (2013) Interlaboratory study for coral Sr/Ca and other element/Ca ratio measurements. *Geochem. Geophys. Geosyst.* **14**(9), 3730–3750.

Heuser A., Eisenhauer A., Böhm F., Wallmann K., Gussone N., Pearson P. N., Nägler Th. F. and Dullo W. Chr. (2005) Calcium isotope (d44/40Ca) variations of Neogene planktonic foraminifera. *Paleoceanography* **20**.

Heuser A., Eisenhauer A., Gussone N., Bock B., Hansen B. T. and Nägler Th. F. (2002) Measurement of calcium isotopes (ð44Ca) using a multicollector TIMS technique. *Int. J. Mass Spectrom.* **220**, 385–397.

Holland H. D., Borcsik M., Munoz J. and Oxburgh U. M. (1963) The co-precipitation of Sr^{2+} with aragonite and of Ca^{2+} with strontianite between 90 and 100 °C. *Geochim. Cosmochim. Acta* **27**, 957–977.

Irving H. and Williams R. J. P. (1953) The stability of transition metal complexes. *J. Chem. Soc.*, 3192–3210.

Kim S.-T., Gebbinck C. K., Mucci A. and Coplen T. B. (2014) Oxygen isotope systematics in the aragonite–CO_2–H_2O–NaCl system up to 0.7 mol/kg ionic strength at 25 °C. *Geochim. Cosmochim. Acta* **137**, 147–158.

Kinsman D. J. J. and Holland H. D. (1969) The co-precipitation of cations with $CaCO_3$. The co-precipitation of Sr^{2+} with aragonite between 16 and 96 °C. *Geochim. Cosmochim. Acta* **33**, 1–17.

Kelleher I. J. and Redfern S. A. T. (2002) Hydrous calcium magnesium carbonate, a possible precursor to the formation of sedimentary dolomite. *Mol. Simul.* **28**(6–7), 557–572.

Lemarchand D., Wasserburg G. J. and Papanastassiou A. (2004) Rate-controlled calcium isotope fractionation in synthetic calcite. *Geochim. Cosmochim. Acta* **68**(22), 4665–4678.

Kisakürek B., Eisenhauer A., Böhm F., Garbe-Schönberg D. and Erez J. (2008) Controls on shell Mg/Ca and Sr/Ca in cultured planktonic foraminiferan, G/lobigerinoides ruber/(white). *Earth Planet. Sci. Lett.* **273**, 260–269. http://dx.doi.org/10.1016/j.epsl.2008.06.026.

Krabbenhöft A., Fietzke J., Eisenhauer A., Liebetrau V., Böhm F. and Vollstaedt H. (2009) Determination of radiogenic and stable strontium isotope ratios $^{87}Sr/^{86}Sr$; $\Delta^{88}/^{86}Sr$ by thermal ionization mass spectrometry applying an $^{87}Sr/^{84}Sr$ double spike. *J. Anal. Atom. Spectrom.* **24**(9), 1267–1271.

Millero F. J. (1995) Thermodynamics of the carbon dioxide system in the oceans. *Geochim. Cosmochim. Acta* **59**, 661–677.

Meibom A., Cuif J.-P., Hillion F., Constantz B. R., Juillet-Leclerc A., Dauphin Y., Watanabe T. and Dunbar R. B. (2004) Distribution of magnesium in coral skeleton. *Geophys. Res. Lett.*, 31.

Morse J. W. and Mackenzie F. T. (1990) *Geochemistry of Sedimentary Carbonates*. Elsevier Science Publisher B.V, Amsterdam.

Morse J. W., Arvidson R. S. and Lüttge A. (2007) Calcium carbonate formation and dissolution. *Chem. Rev.* **107**, 342–381.

Niedermayr A., Köhler S. J. and Dietzel M. (2013) Impacts of aqueous carbonate accumulation rate, magnesium and polyaspartic acid on calcium carbonate formation (6–40 °C). *Chem. Geol.* **340**, 105–120.

Petrou A. L. and Terzidaki A. (2014) Calcium carbonate and calcium sulfate precipitation, crystallization and dissolution: evidence for the activated steps and the mechanisms from the enthalpy and entropy of activation values. *Chem. Geol.* **381**, 144–153.

Rodriguez-Cruz S. E., Jockusch R. A. and Williams E. R. (1999) Binding energies of hexahydrated alkaline earth metal ions, $M^{2+}(H_2O)_6$, M = Mg, Ca, Sr, Ba: evidence of isomeric structures for magnesium. *J. Am. Chem. Soc.* **121**(9), 1986–1987.

Rohlf J. W. (1994) *Modern Physics from Alpha to Z^0*. Wiley.

Romanek C. S., Morse J. W. and Grossman E. L. (2011) Aragonite kinetics in dilute solutions. *Aquat. Geochem.* **17**, 339–356.

Scherer M. and Seitz H. (1980) Rare-earth element distribution in Holocene and Pleistocene corals and their distribution during diagenesis. *Chem. Geol.* **28**, 279–289.

Seward R. P. (1954) The complexing of hydrazine with calcium ion as determined by distribution measurements. *J. Am. Chem. Soc.* **76**(19), 4850–4852.

Smith S. V., Buddemeier R. W., Redalje R. C. and Houck J. E. (1979) Strontium-calcium thermometry in coral skeletons. *Science* **204**(4391), 404–407.

Sun W., Jayaraman S., Chen W., Persson K. A. and Ceder G. (2015) Nucleation of metastable aragonite $CaCO_3$ in seawater. *Appl. Phys. Sci.* **112**(11), 3199–3204.

Tang J., Köhler S. J. and Dietzel M. (2008) Sr^{2+}/Ca^{2+} and $^{44}Ca/^{40}Ca$ fractionation during inorganic calcite formation: I. Sr incorporation. *Geochim. Cosmochim. Acta* **72**, 3718–3732.

Usdowski H. E. (1975) *Fraktionierung der Spurenelemente bei der Kristallisation*. Springer-Verlag, Berlin, Heidelberg, p. 104.

Weber J. N. (1973) Incorporation of strontium into reef coral skeletal carbonate. *Geochim. Cosmochim. Acta* **37**(9), 2173–2190.

Wombacher F., Eisenhauer A., Böhm F., Gussone N., Regenberg M., Dullo W. C. and Rüggeberg A. (2011) Magnesium stable isotope fractionation in marine biogenic calcite and aragonite. *Geochim. Cosmochim. Acta* **75**(19), 5797–5818.

Zeebe R. E. and Wolf-Gladrow D. A. (2001) *CO2 in Seawater: Equilibrium, Kinetics. Isotopes*. Elsevier, Amsterdam.

Associate editor: Andrew D. Jacobson